https://ntrs.nasa.gov/search.jsp?R=19890013677 2020-03-20T03:17:04+00:00Z

PB89-127831

Hazard Index Calculation for May 31, 1984 Microburst at Erie, Colorado

(U.S.) National Oceanic and Atmospheric Administration, Boulder, CO

Prepared for

National Aeronautics and Space Administration
Hampton, VA

Oct 88

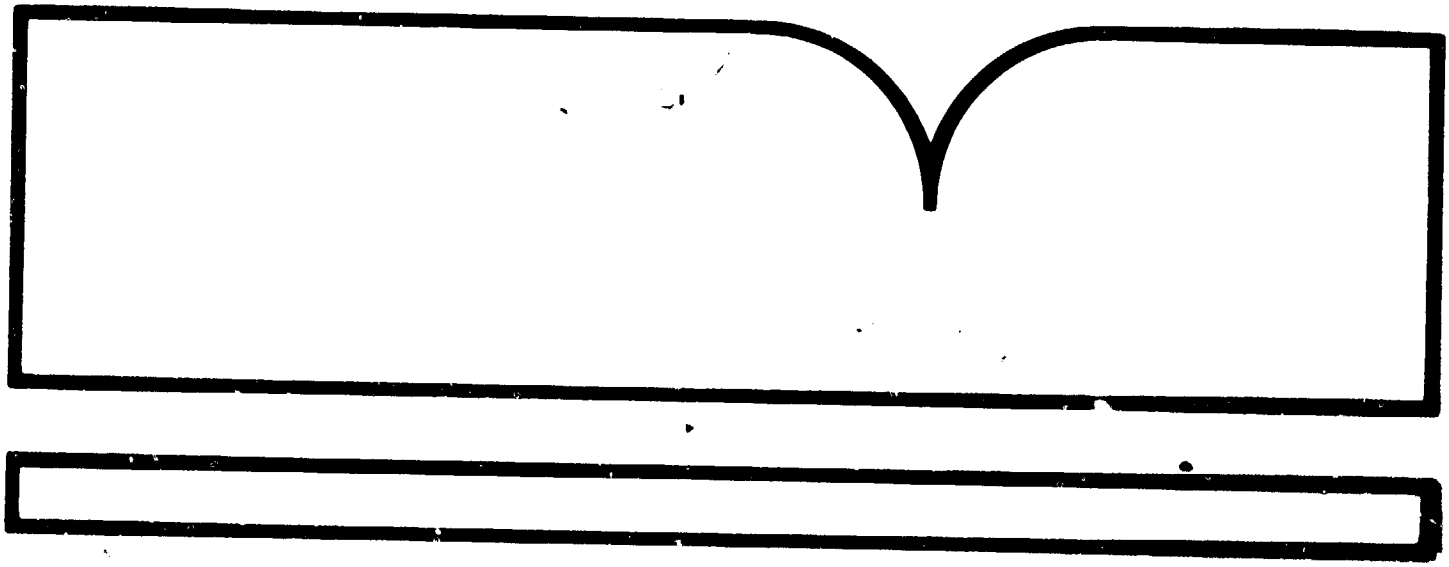

U.S. Department of Commerce
National Technical Information Service
NTIS

BIBLIOGRAPHIC INFORMATION

PB89-127831

Report Nos: NOAA-TM-ERL-WPL-155

Title: Hazard Index Calculation for May 31, 1984 Microburst at Erie, Colorado.

Date: Oct 88

Authors: R. A. Kropfli.

Performing Organization: National Oceanic and Atmospheric Administration, Boulder, CO. Wave Propagation Lab.

Sponsoring Organization: *National Aeronautics and Space Administration, Hampton, VA. Langley Research Center.

Type of Report and Period Covered: Technical memo.,

Supplementary Notes: Portions of this document are not fully legible. Sponsored by National Aeronautics and Space Administration, Hampton, VA. Langley Research Center.

NTIS Field/Group Codes: 55B, 51B

Price: PC A04/MF A01

Availability: Available from the National Technical Information Service, Springfield, VA. 22161

Number of Pages: 54p

Keywords: *Atmospheric motion, *Hazards, *Boundary layer, *Aircraft, Dissipation, Flight paths, Kinetic energy, Doppler radar, Damage, Wind pressure, *Microburst, PHOENIX 2 boundary layer experiment.

Abstract: The two x-band Doppler radars, operated by the NOAA Wave Propagation Laboratory, were used to collect high resolution data within a small, benign-looking microburst during the PHOENIX II boundary layer experiment. The lowest 2.5 km of the microburst was observed throughout its development and dissipation over a 15 minute period. These observations presented an excellent opportunity to compute a quantitative threat to a hypothetical aircraft whose flight track would carry it through the microburst. The hazard index is based on the kinetic energy loss to the aircraft that would be produced by the microburst; it is a function of the vertical air motion, horizontal spatial derivatives of the wind field, and the assumed aircraft air speed and direction. Indices were computed and plotted for all eight volume scans and peak values were observed to be sufficiently high to present a significant hazard to an aircraft.

PB89-127831

NOAA Technical Memorandum ERL WPL-155

HAZARD INDEX CALCULATION FOR MAY 31, 1984 MICROBURST AT ERIE, COLORADO

R. A. Kropfli

Wave Propagation Laboratory
Boulder, Colorado
October 1988

noaa NATIONAL OCEANIC AND ATMOSPHERIC ADMINISTRATION / Environmental Research Laboratories

REPRODUCED BY
U.S. DEPARTMENT OF COMMERCE
NATIONAL TECHNICAL INFORMATION SERVICE
SPRINGFIELD, VA. 22161

N O T I C E

THIS DOCUMENT HAS BEEN REPRODUCED FROM THE BEST COPY FURNISHED US BY THE SPONSORING AGENCY. ALTHOUGH IT IS RECOGNIZED THAT CERTAIN PORTIONS ARE ILLEGIBLE, IT IS BEING RELEASED IN THE INTEREST OF MAKING AVAILABLE AS MUCH INFORMATION AS POSSIBLE.

NOAA Technical Memorandum ERL WPL-155

HAZARD INDEX CALCULATION FOR MAY 31, 1984 MICROBURST AT ERIE, COLORADO

R. A. Kropfli

Wave Propagation Laboratory
Boulder, Colorado
October 1988

UNITED STATES
DEPARTMENT OF COMMERCE

C.William Verity
Secretary

NATIONAL OCEANIC AND
ATMOSPHERIC ADMINISTRATION

William E. Evans
Under Secretary for Oceans
and Atmosphere/Administrator

Environmental Research
Laboratories

Vernon E. Derr,
Director

1-cl

NOTICE

Mention of a commercial company or product does not constitute an endorsement by NOAA Environmental Research Laboratories. Use for publicity or advertising purposes of information from this publication concerning proprietary products or the tests of such products is not authorized.

For sale by the National Technical Information Service, 5285 Port Royal Road
Springfield, VA 22161

PREFACE

The NOAA Wave Propagation Laboratory in Boulder, Colorado, has been contracted by NASA Langley Research Center to compute hazard indices from dual-Doppler radar data taken during the PHOENIX II boundary layer experiment. This final report summarizes the results of these calculations.

CONTENTS

1. INTRODUCTION 1

2. DISCUSSION 1

3. REFERENCES 5

APPENDIX I—Reprint of: A Microburst Observed by High-Resolution Dual-Doppler Radar 7

APPENDIX II—Hazard Index Plots 15

APPENDIX III—Tape Format 47

Preceding page blank

HAZARD INDEX CALCULATION FOR MAY 31, 1984 MICROBURST AT ERIE, COLORADO

ABSTRACT. The two x-band Doppler radars, operated by the NOAA Wave Propagation Laboratory, were used to collect high resolution data within a small, benign-looking microburst during the PHOENIX II boundary layer experiment. The lowest 2.5 km of the microburst was observed throughout its development and dissipation over a 15 minute period. These observations presented an excellent opportunity to compute a quantitative threat to a hypothetical aircraft whose flight track would carry it through the microburst. This hazard index is based on the kinetic energy loss to the aircraft that would be produced by the microburst; it is a function of the vertical air motion, horizontal spatial derivatives of the wind field, and the asssumed aircraft air speed and direction. Indices were computed and plotted for all eight volume scans and peak values were observed to be sufficiently high to present a significant hazard to an aircraft even though the virga-produced microburst was visually unimpressive.

1. INTRODUCTION

During the PHOENIX II convective boundary layer experiment conducted during May and June of 1984, the two x-band Doppler radars operated by the NOAA/Wave Propagation Laboratory documented the evolution of a small microburst. This microburst was located 30 km NW of Denver's Stapleton International Airport and was one of a family of microbursts that were evident in the area on that day. Twenty minutes prior to this event another microburst was believed to have been the cause of significant damage to UAL Flight 633 upon takeoff from Stapleton (NTSB, 1985).

The dual-Doppler radar synthesis performed with this data set is of excellent resolution, both temporally and spatially, because of the short radar baseline (13 km) and scan volume repetition cycle (100 s). A description of the wind fields synthesized on a 150 m grid at 100 m intervals is given by Kropfli (1986) and is provided in Appendix I.

The Hazard Index, an aircraft-specific measure of the threat for a given wind shear condition (Bowles and Targ, 1988), has been computed for this data set. Contour plots of the Hazard Index have been plotted for the lowest horizontal plane for each of eight volume scans, and they are included here in Appendix II. Four flight directions were assumed. These data have also been recorded on two ASCII formatted tapes that are included along with this report.

2. DISCUSSION

The Hazard Index, as defined by Bowles and Targ (1988), is the loss in available excess thrust-to-weight ratio of an aircraft due to vertical air motions and horizontal windshear. It is expressed as follows:

$$F = (V/g)du/dx - w/V$$

where V is the airspeed, g is acceleration due to gravity, du/dx is the horizontal gradient of the horizontal wind along the direction of the flight path, and w is the vertical component of the wind. Their analysis shows that the potential rate of climb can be expressed as

$$dh/dt = \{[T - D]/W - F\}V$$

where T is the aircraft thrust, D is the drag, and W is the aircraft weight. From this expression the Hazard Index is seen to be the tangent of the difference between the actual glide slope from the desired glide slope caused by vertical air motion and horizontal wind shear. Values of F in the neighborhood of .10 to .15 are believed to be reasonable threshold levels above which an aircraft is in danger.

For this study four flight directions were assusmed for the 31 May microburst; *toward* the north, east, south, and west and the corresponding Hazard Indices are expressed as FN, FE, FS, and FW respectively. Expressions for the Hazard Index in the four directions computed here are given as follows:

$$FN = (V/g)dv/dy - w/V$$

$$FS = -(V/g)dv/dy - w/V$$

$$FE = (V/g)du/dx - w/V$$

$$FW = -(V/g)du/dx - w/V$$

where u and v are the synthesized horizontal winds along the x (east) and y (north) axes respectively, w is the synthesized vertical air motion (positive upward), and V is the specified aircraft airspeed (140 kt). Horizontal gradients of the wind were computed with a three point central difference method applied to wind fields synthesized from the 31 May dual-Doppler radar measurements (Kropfli, 1986).

The above four Hazard Indices were computed for the four lowest horizontal levels of each of the eight processed radar volumes. These levels are at 75 m, 225 m, 375 m, and 525 m above ground. The ASCII formatted tapes and the contours provided in Appendix II include the fields FN, FS, FE, and FW along with all necessary housekeeping information. Table 1 indicates the start times (MST) of each of the eight volumes that were processed.

Table 1. Volume start times

Volume Number	Time of Start (MST)
1	1247:23
2	1249:03
3	1250:43
4	1252:23
5	1254:04
6	1255:44
7	1257:24
8	1259:04

Table 2 below lists the peak indices for all eight volumes as a function of height. It is apparent from the table that indices for this microburst would have been hazardous to aircraft approaching or taking off in some directions since it produced values that often exceeded .10, especially for the indices FE and FN. Values exceeding .12 were observed for FN near the surface for volumes 5 and 6 and also for FE, though only at altitudes of 225 m and above. The largest value observed was .15 for volume 6 at the lowest level for an approach or departure toward the north.

This microburst exhibits a strong asymmetry, with flight paths toward the east and the north having peak values nearly three times greater than values observed for the other directions. Flight paths through this microburst toward the north or the east would clearly be much more hazardous than flights toward the west or south.

The height dependence of the maxima varied differently with flight direction; FE peak values were generally increasing with height and FN was more nearly constant. The temporal behavior of the peak hazard index was somewhat erratic but generally the highest values were found in the three scans centered around 1254:04, as would be expected from a perusal of the synthesized wind fields (Kropfli, 1986).

The magnetic tape provided to NASA/Langley is card image format with 80 ASCII characters/record. Along with the data discussed above, the tape contains important housekeeping information such as the grid specifications, field names, radar coordinates, and volume start and end times. A description of the tape format is also provided in Appendix III along with the housekeeping information written to tape for all eight volumes.

Table 2. Peak hazard index as a function of time, direction and height

Index	Volume Number	Height (M AGL)			
		75	225	375	525
FN	1	.081	.063	.057	.070
	2	.084	.063	.065	.079
	3	.091	.087	.084	.067
	4	.098	.098	.128	.134
	5	.120	.119	.105	.097
	6	.152	.118	.096	.099
	7	.076	.083	.089	.103
	8	.071	.061	.070	.068
FS	1	.055	.033	.039	.055
	2	.053	.034	.045	.056
	3	.053	.044	.061	.089
	4	.049	.049	.063	.079
	5	.065	.072	.078	.113
	6	.065	.059	.092	.105
	7	.057	.070	.081	.100
	8	.050	.055	.068	.085
FE	1	.057	.054	.058	.057
	2	.075	.065	.076	.102
	3	.071	.096	.115	.121
	4	.096	.110	.128	.149
	5	.082	.121	.140	.141
	6	.095	.091	.113	.137
	7	.095	.086	.115	.129
	8	.070	.089	.100	.092
FW	1	.040	.038	.039	.046
	2	.040	.035	.044	.050
	3	.039	.049	.045	.064
	4	.048	.053	.053	.059
	5	.039	.044	.059	.068
	6	.058	.060	.075	057
	7	.057	.048	.046	.058
	8	.048	.041	.043	.055

3. REFERENCES

Bowles, R., and R. Targ, 1988: Windshear detection and avoidance: Airborne systems and perspective. 16th Congress of the International Council of the Aeronautical Sciences, Jerusalem, Israel.

Kropfli, R.A., 1986: A microburst observed by high-resolution dual-Doppler radar. Preprints 23rd Conf. on Radar Meteorology, American Meteorological Society. J109–J112.

NTSB, 1985: UAL Flight 663 Aircraft Accident Report, Denver, CO, May 31, 1984. NTSB/AAR85/05.

APPENDIX I

Reprint of: A Microburst Observed by High-Resolution Dual-Doppler Radar

Preceding page blank

Reprinted from the preprint volumes for the 23rd Conference on Radar Meteorology and the Conference on Cloud Physics, Sept. 22-26, 1988, Snowmass, Colo. Published by the American Meteorological Society, Boston, Mass.

J13.5

A MICROBURST OBSERVED BY HIGH-RESOLUTION DUAL-DOPPLER RADAR

R. A. Kropfli
NOAA/ERL/Wave Propagation Laboratory
Boulder, Colorado 80303

1. INTRODUCTION

The Phoenix II convective boundary layer (CBL) experiment was conducted near the Boulder Atmospheric Observatory (BAO) instrumented tower during the summer of 1984. The experiment, a collaborative effort between the University of Oklahoma, National Oceanic and Atmospheric Administration (NOAA), and National Center for Atmospheric Research (NCAR), addressed the small-scale structure of the CBL with Doppler radar, instrumented aircraft, and surface measurements. Scan procedures and the 13 km radar separation optimized measurements of the small-scale and short-lived eddies present in the dry CBL. This experimental design was also suitable for documenting microbursts, which often develop and decay within a 10 min period and have downdrafts that are as small as 1 km in diameter just above the surface (Wilson et al., 1984; Fujita, 1981). Two adjacent areas of dual-Doppler radar coverage were established: one formed by the two NCAR C-band radars and the other formed by the two NOAA/WPL X-band radars. The 31 May microburst discussed here was centrally located within the scan area of the NOAA radars, and these two radars are used in the analysis.

There were three confirmed reports of microbursts on this day during which virga and many small rainshafts were observed; it is suspected that a large number of such events were occurring throughout the region. Confirmation of one of these events came from a jetliner departing from Stapleton Airport about 30 km to the southeast of the Phoenix II measurement area. As a result of a 10 m s^{-1} loss of airspeed during acceleration down the runway, the aircraft failed to clear a 5-m-high radio beacon located 300 m beyond the end of the runway resulting in major damage to the fuselage. The loss of airspeed was later determined to be the result of a moderately strong microburst that impacted the runway at around 1235 MST (NTSB, 1985). Fortunately, the aircraft climbed out of danger and returned safely to Stapleton with no injury or loss of life.

The event documented here took place about 20 minutes later near the BAO, and a third microburst was evident in the anemometer records at the BAO several hours later (Bedard, personal communication). This near-tragedy at Stapleton along with other well-documented aircraft accidents (Fujita and Byers, 1977) underscores the importance of finding reliable precursor signatures in Doppler radar observations of microbursts. Several features of the 31 May microburst are apparent in the radar data that might be useful in identifying microbursts several minutes before the outflow reaches its maximum intensity at the surface.

2. ENVIRONMENTAL CONDITIONS

The 12 Z (0600 MST) Denver sounding shown in Fig. 1 suggests that the likelihood of microbursts occurring on this day was high. Note especially the high lapse rate (8.9 deg/km) just below the 500 mb level, the high relative humidity above 600 mb, and the relatively dry layer below 600 mb. These features have been associated with the occurrence of microbursts (Fujita et al., 1983; Bedard and LeFebvre, 1986). The NCAR instrumented King Air aircraft had been making soundings within and near the area of dual-Doppler radar observations (Hildebrand, personal communication); the potential temperature and mixing ratio profiles from the sounding at 1236 MST are shown in Fig. 2. A well-mixed layer is seen below 2 km AGL, and slightly stable air is present from 2 km to 3 km AGL, the highest level flown. (All heights are AGL.) The melting level was found to be at 2.8 km and cloud base was at 3.8 km. Figure 3 shows the mean wind profile derived from the dualDoppler analysis at 1250:45 and indicates moderate shear toward the northeast at about 0.003 s^{-1}. The mean profiles of wind, stability, and relative humidity seem critical to the overall physical structure of this event.

3. PHYSICAL CHARACTERISTICS

Figure 4 indicates that the microburst near the BAO was in an ideal location relative to the two NOAA X-band radars. At the time of the incident at Stapleton, these two radars were being used in high resolution observations of the

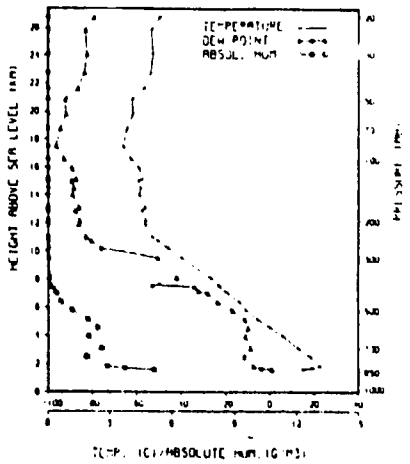

Figure 1. Temperature and humidity profiles from the NWS morning radiosonde at Denver on 31 May 1984.

Preceding page blank

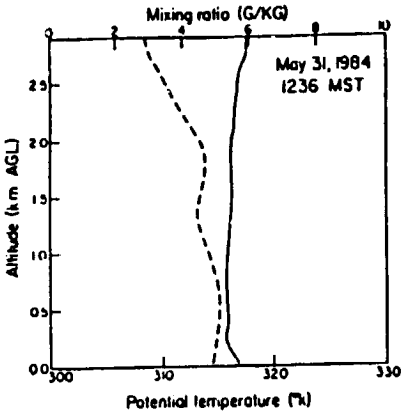

Figure 2. Potential temperature (solid) and mixing ratio (dashed) profiles from the NCAR King Air aircraft taken near the BAO at 1236 MST on 31 May 1984.

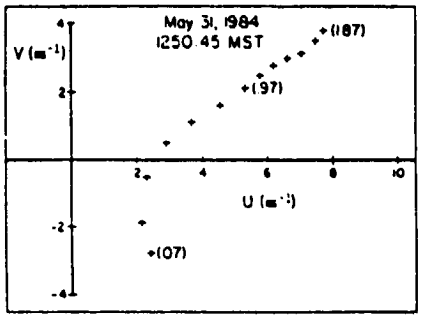

Figure 3. Hodograph obtained from the Doppler radar derived wind field at 1250:45 MST on 31 May 1984. Height AGL in km shown in parentheses.

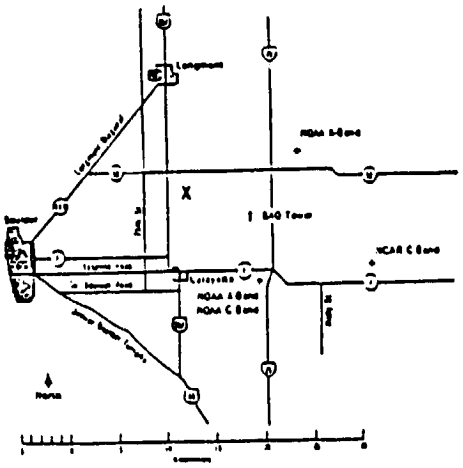

Figure 4. Phoenix II experimental layout showing approximate location of the microburst, indicated by the X.

CBL to a height of 2.5 km and with a scan cycle time of 100 s. These measurements permitted use of the 150 m grid spacing shown in Figs. 5 to 9. A 0.7 μs pulse width and a beam separation of 0.7 deg in azimuth were used in these measurements.

Figure 5 shows the east-west cross section through the core of the microburst, the result of a synthesis of the dual-Doppler radar data taken at 1254:04. (In all the flow fields shown here the volume mean of approximately 5.2 m s^{-1} to the ENE was removed to display the flow features more clearly.) It is apparent that the downdraft has its source region above 2.5 km AGL. A maximum downward air motion of nearly 8 m s^{-1} occurs at about 700 m.

The sequence of horizontal views at z = 75 m in Fig. 6 shows the rapid development of the divergent outflow near the surface at 100 s intervals. Figure 6c shows the surface outflow at maximum intensity when a peak divergence of 0.02 s^{-1} was observed. The maximum surface reflectivity of 39 dBZ occurred 5 min earlier at 1250 and decreased gradually to 36 dBZ by 1256.

A comparison of Fig. 7, showing the horizontal flow at 375 m, with the low level flow at the same time (1252:23) in Fig. 6a suggests that the divergent outflow was readily observable above the surface nearly 200 s before it reached its maximum at the surface. In this case horizontal divergence at a height of several hundred meters might have been a precursor of strong, potentially dangerous outflows at the surface. It is also conceivable that a single radar, appropriately located relative to the microburst might have detected this precursor to the surface outflow.

A second precurser, midlevel convergence, is suggested by Fig. 8. These data were taken at 1250:43 and at a height of nearly 1.9 km. It is

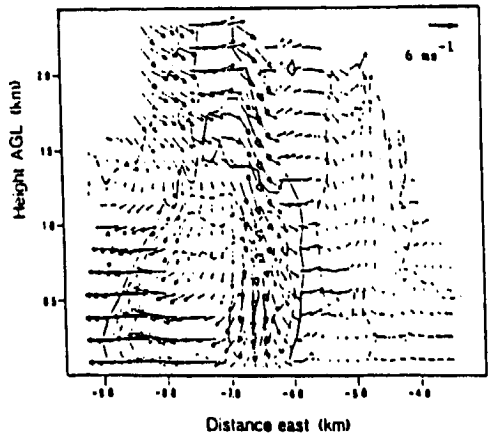

Figure 5. East-west cross-section of dual-Doppler eddy wind field through core of the microburst at 1254:04 MST. The cross section is taken 3.0 km north of the BAO. The solid contour represents the 9.5 dBZ reflectivity, and the dashed lines are at 5.5 dB increments.

Reproduced from
best available copy.

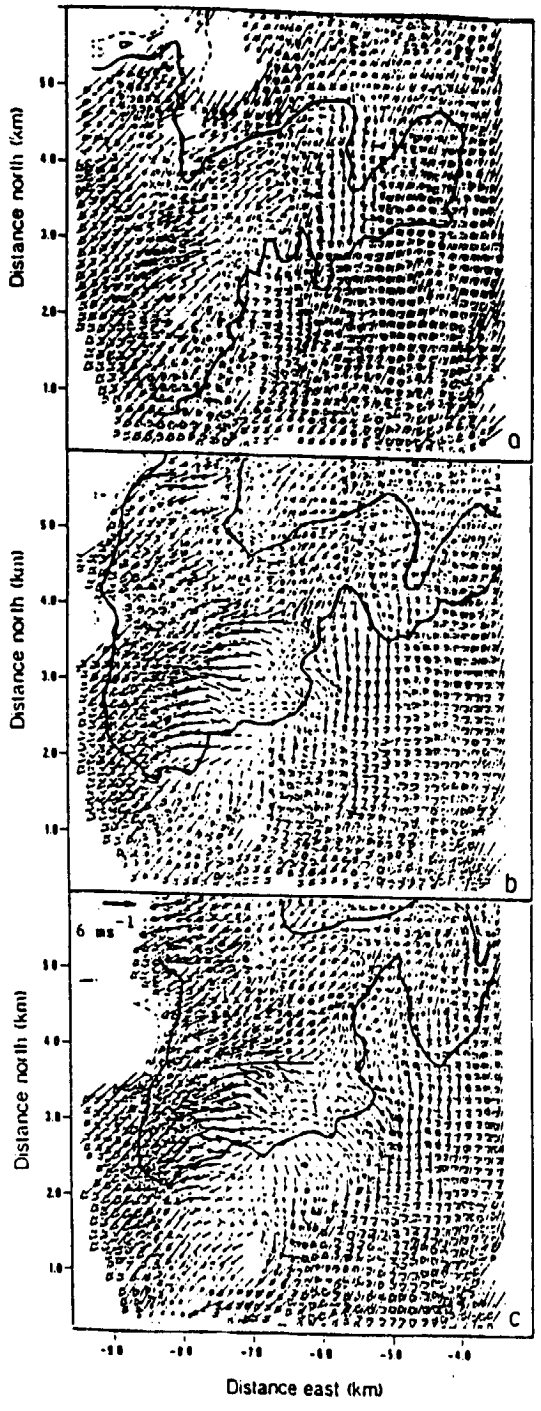

Figure 6. The horizontal eddy wind field at z = 75 m. Arrows are scaled as in Fig. 5 and reflectivity contours are approximately the same as in Fig. 5. (a) 1252:23 MST; (b) 1254:04 MST; (c) 1255:44 MST.

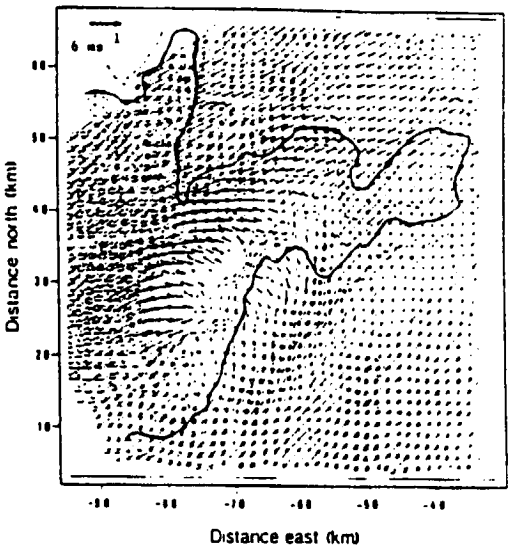

Figure 7. As in Fig. 6a except at z = 375 m.

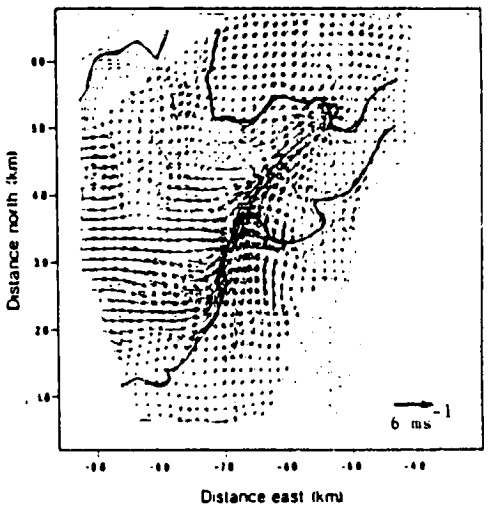

Figure 8. As in Fig. 6a except at z = 1.9 km and at 1250:43 MST.

likely that air near the 2 km level was entrained into the downdraft that had been initiated by precipitation from the cloud above 4.8 km. Convergence near the bottom of a slightly stable layer may indicate that strong outflows will soon be found at the surface. In this case the convergence at 2 km preceeded the maximum divergence at the surface by nearly 5 min. Table 1 summarizes some of the properties of the microburst during its time of maximum outflow at 75 m.

An unexpected feature of these observations is the movement of the reflectivity maximum away from the peak downdraft region near the surface. Figure 9 indicates this with every other scan from 1250:43 to 1257:24 being shown; i.e., the samples in the figure are at 200 s intervals. The regions enclosed by solid con-

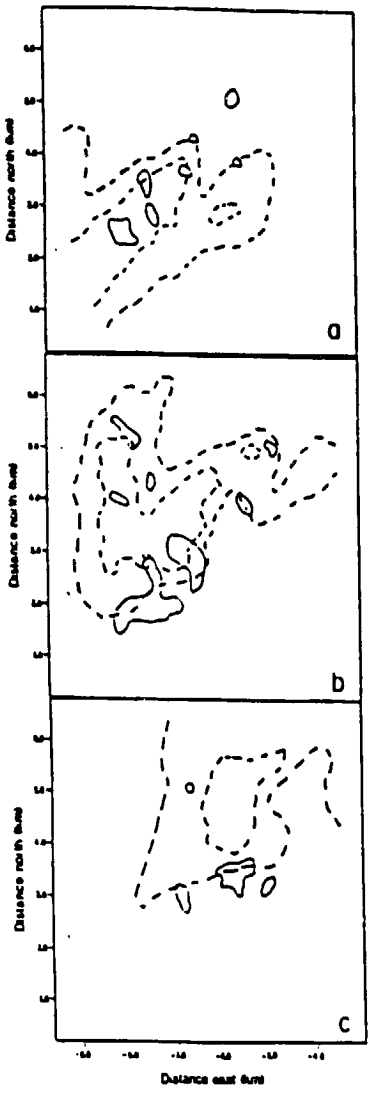

Figure 9. Reflectivity contours at 10 dBZ (dashed) and 24 dBZ (dashed) and w = -1.0 m s^{-1} (solid) at 1250:43 MST and at z = 75 m. (a) 1250:43 MST; (b) 1254:04 MST; (c) 1257:24 MST.

Table 1. Summary of microburst properties at (1255:44 MST) time of maximum low-level divergence

Peak divergence at 75 m:	2.1×10^{-2} s^{-1}
Peak reflectivity at 75 m:	36 dBZ
Peak downdraft and height:	6.5 m s^{-1}, .8 km AGL
Area with DIV > 10^{-2} s^{-1} at 75 m:	.4 km^2
Mean flow in sample volume:	5.2 m s^{-1} from WSW
Time after first appearance of convergence at ~2 km:	~5 min
Time after first appearance of divergence at ~.4 km	~3 min

tours indicate w < -1 m^{-1} and the inner dashed contour encloses reflectivity greater than 24 dBZ. w is the vertical air motion. The sequence clearly shows the motion of the heavier precipitation moving to the northeast while the main downdraft region remains nearly stationary. (The three minor downdrafts in the northwest corner of Fig. 9b appear only briefly and are not thought to be of significance.) Near the end of the observations at 1257:24 the decaying downdraft is located almost entirely outside of the 10 dBZ contour.

The preliminary explanation offered for this unexpected observation is that the downdraft is initiated by light rain, in which case water loading could play a significant role along with the negative buoyancy provided by melting and evaporative cooling. With time, melting and evaporative cooling becomes more dominant on the upshear (southwest) side of the precipitation shaft. In effect the source region for the downdraft moves upshear relative to the reflectivity core and into a region of smaller hydrometeors which may be more likely to provide stronger downdrafts as a result of enhanced evaporative cooling (Srivastava, 1985). The reasons for this upshear movement of the source region are not understood, and, unfortunately, the radar observations were not high enough to provide additional insight.

5. SUMMARY

The high resolution Doppler radar observations described here suggest two possible precursor signatures to strong surface outflows associated with microbursts: divergence a few hundred meters above the surface and convergence at heights several kilometers above the surface. We recognize that these links have not been seen before and that the observation of these features prior to surface outflow in this one case merely suggests that future high quality data sets should be examined with this in mind. The separation of the downdraft from the reflectivity core with the passage of time suggests that melting and evaporative cooling play an increasingly dominant role after precipitation loading initiates the downdraft.

6. REFERENCES

Bedard, A., and T. J. LeFebvre, 1986: Surface measurements of gust fronts and microbursts during the Jawa Project: Statistical results and implications for wind shear detection, prediction, and modeling. NOAA Tech. Memo. ERL WPL-135, 112 pp.

Caracena, F., J. McCarthy and J. A. Flueck, 1983: Forecasting the likelihood of microbursts along the Front Range of Colorado. Proc. Thirteenth Conference on Severe Local Storms, Tulsa, Okla., Amer. Meteor. Soc., 261-264.

Fujita, T. T., 1981: Tornadoes and downbursts in the context of generalized planetary scale. J. Atmos. Sci., 38, 1512-1534.

Fujita, T. T., and H. R. Byers, 1977: Spearhead echo and downburst in the crash of an airliner. Mon. Wea. Rev., 105, 129-146.

NTSB, 1985: UAL Flight 663 Aircraft Accident Report, Denver, CO, May 31, 1984. NTSB/AAR85/05.

Srivastava, R. C., 1985: A simple model of evaporatively driven downdraft: Application to microburst downdraft. J. Atmos. Sci., 42, 1004-1023.

Wilson, J. W., R. D. Roberts, C. Kessinger and J. McCarthy, 1984: Microburst wind structure and evaluation of Doppler radar for airport wind detection. J. Clim. Appl. Meteor., 23, 898-915.

APPENDIX II

Hazard Index Plots

Z = 75 m AGL

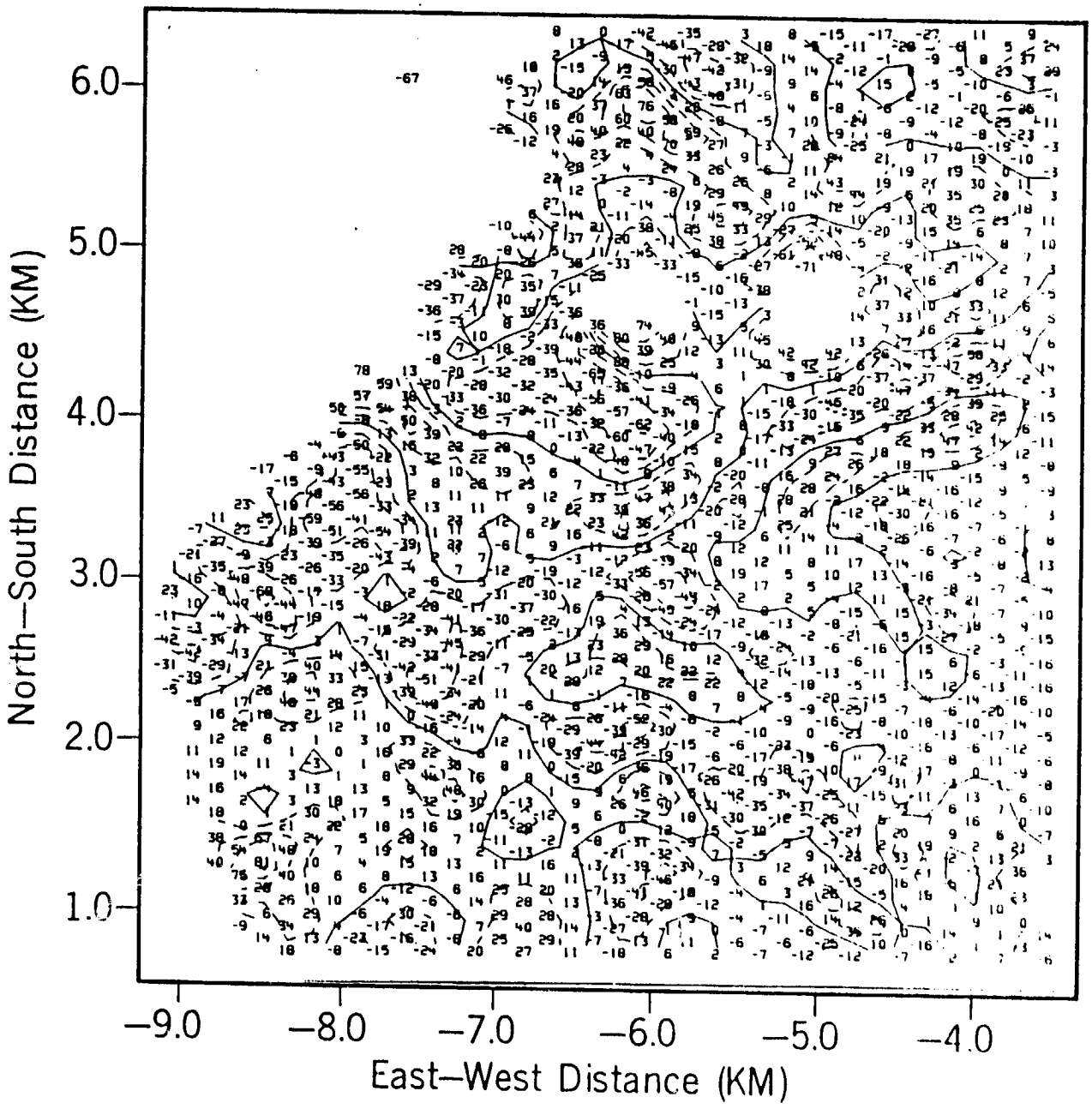

Preceding page blank

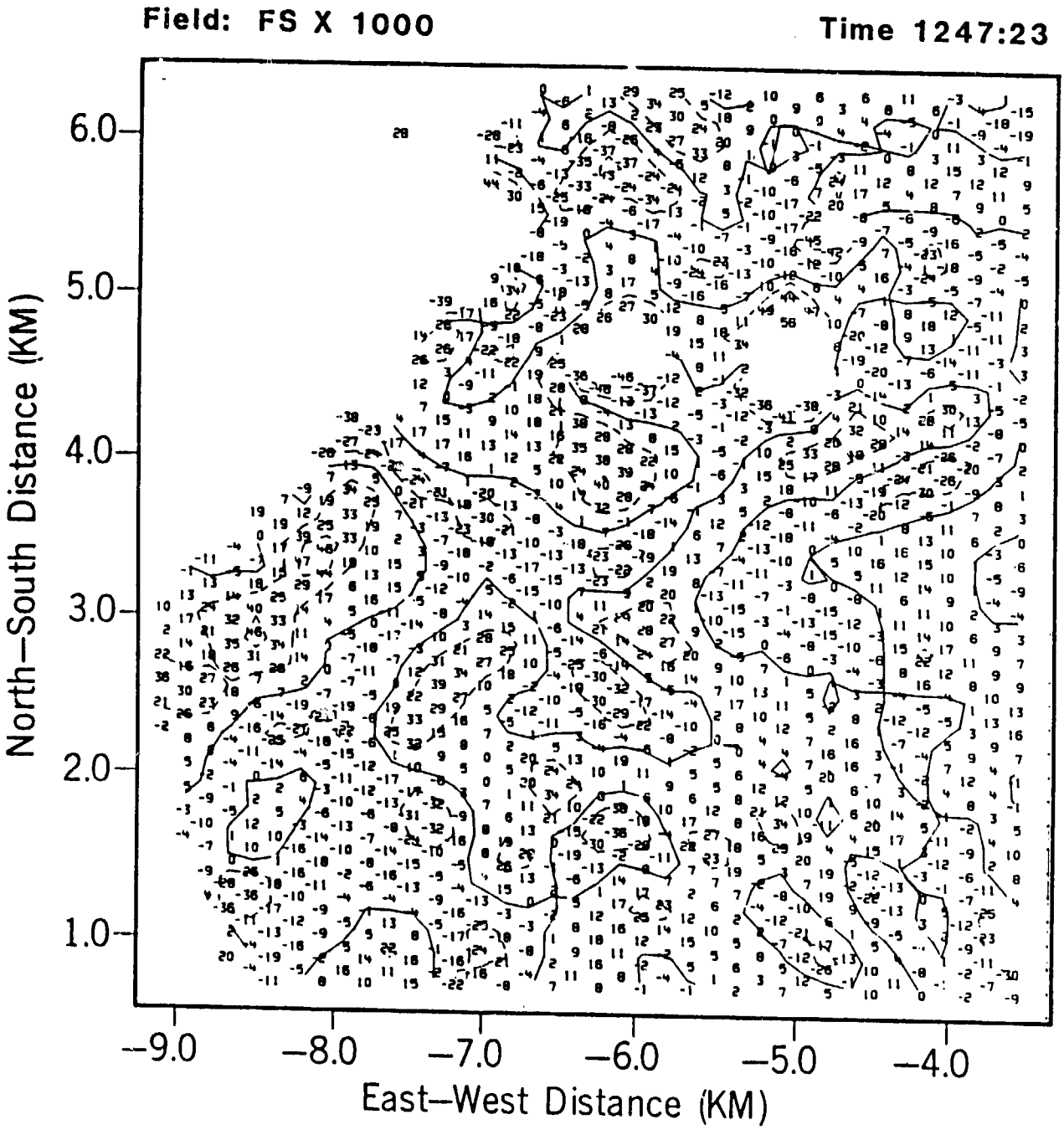
Field: FS X 1000
Time 1247:23
6.0
5.0
4.0
3.0
2.0
1.0
North–South Distance (KM)
–9.0
–8.0
–7.0
–6.0
–5.0
–4.0
East–West Distance (KM)

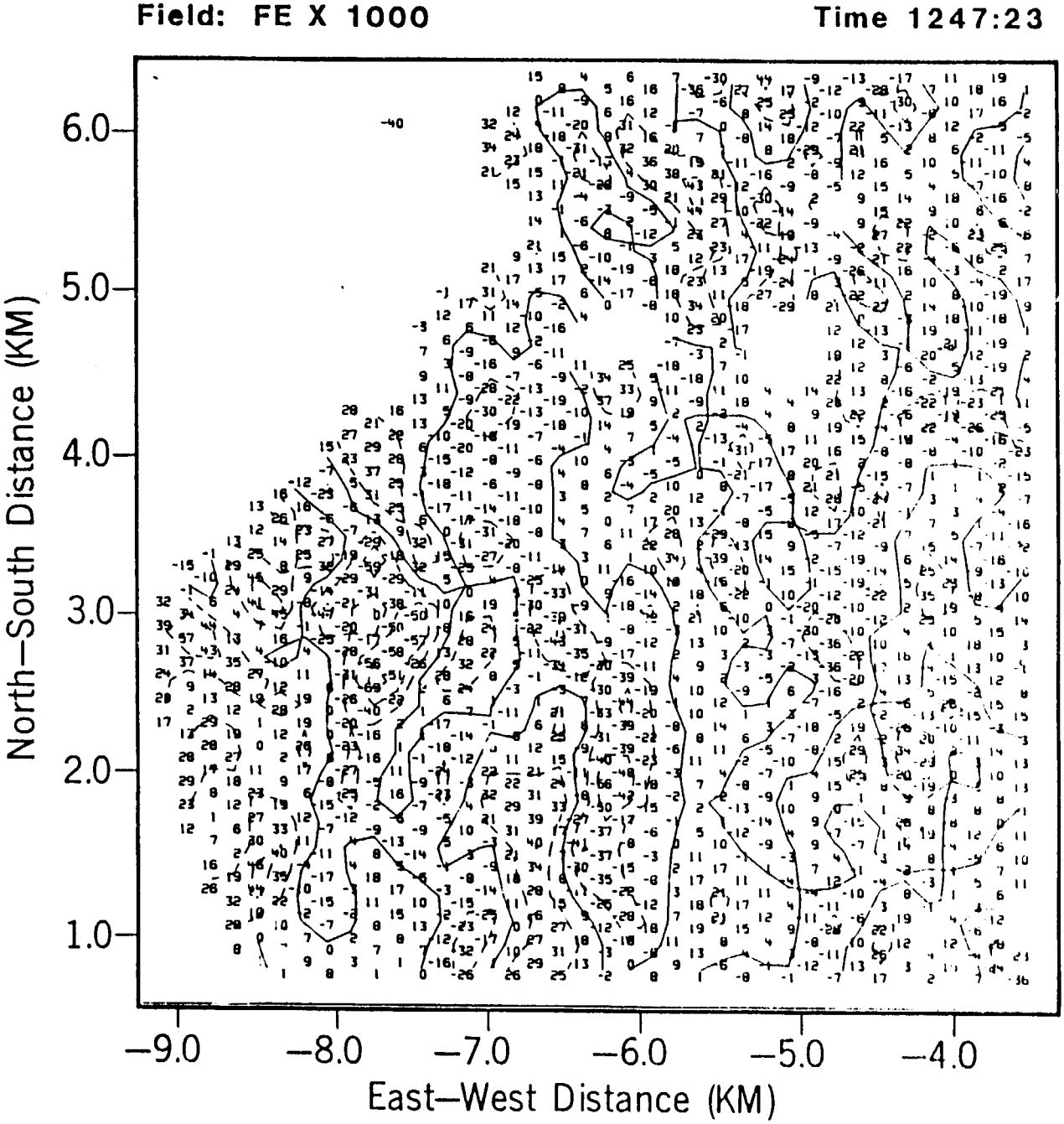
Field: FE X 1000
Time 1247:23
North—South Distance (KM)
6.0
5.0
4.0
3.0
2.0
1.0
−9.0
−8.0
−7.0
−6.0
−5.0
−4.0
East—West Distance (KM)

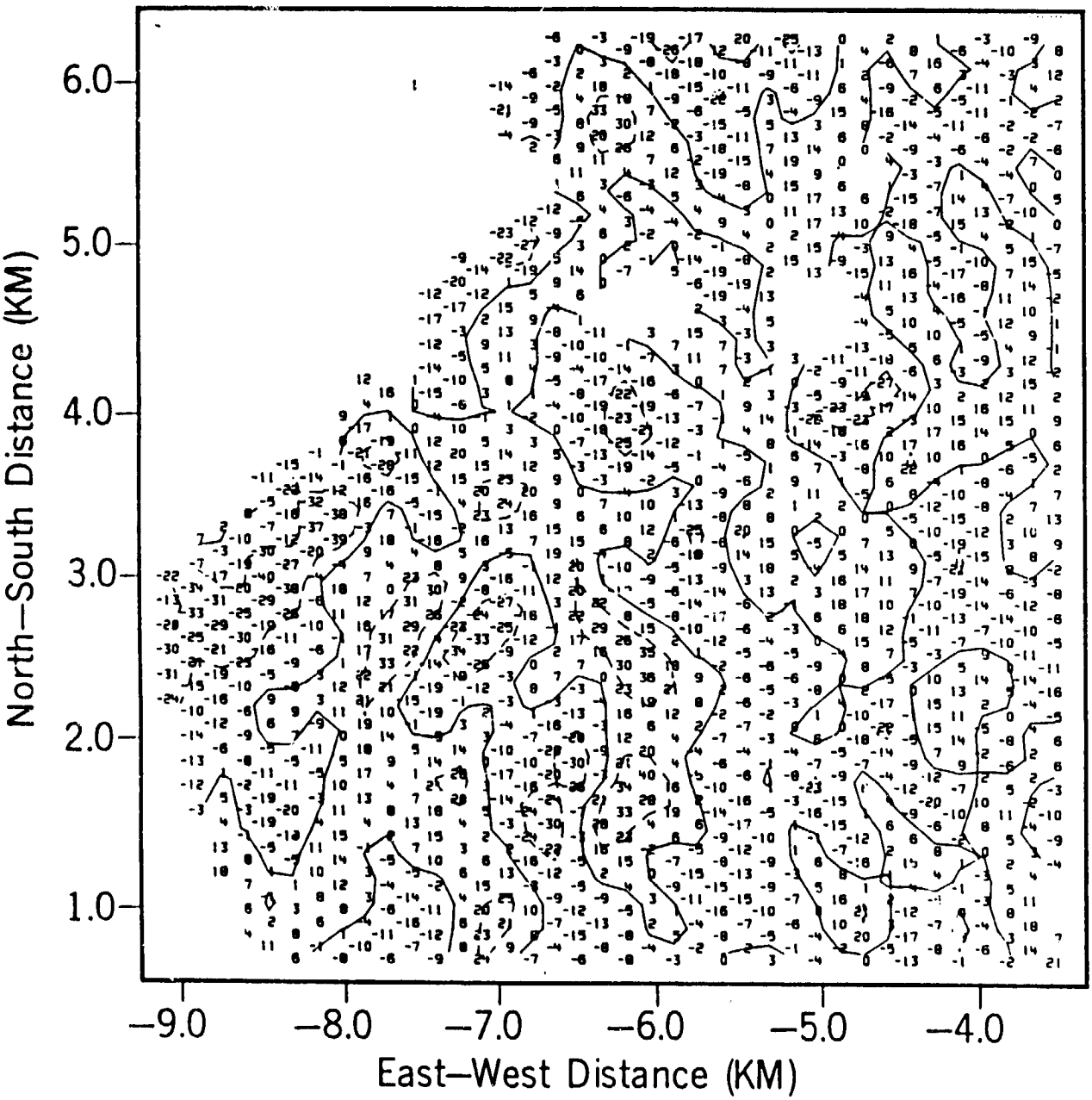
Field: FW X 1000
Time 1247:23
6.0
5.0
4.0
3.0
2.0
1.0
North—South Distance (KM)
—9.0
—8.0
—7.0
—6.0
—5.0
—4.0
East—West Distance (KM)

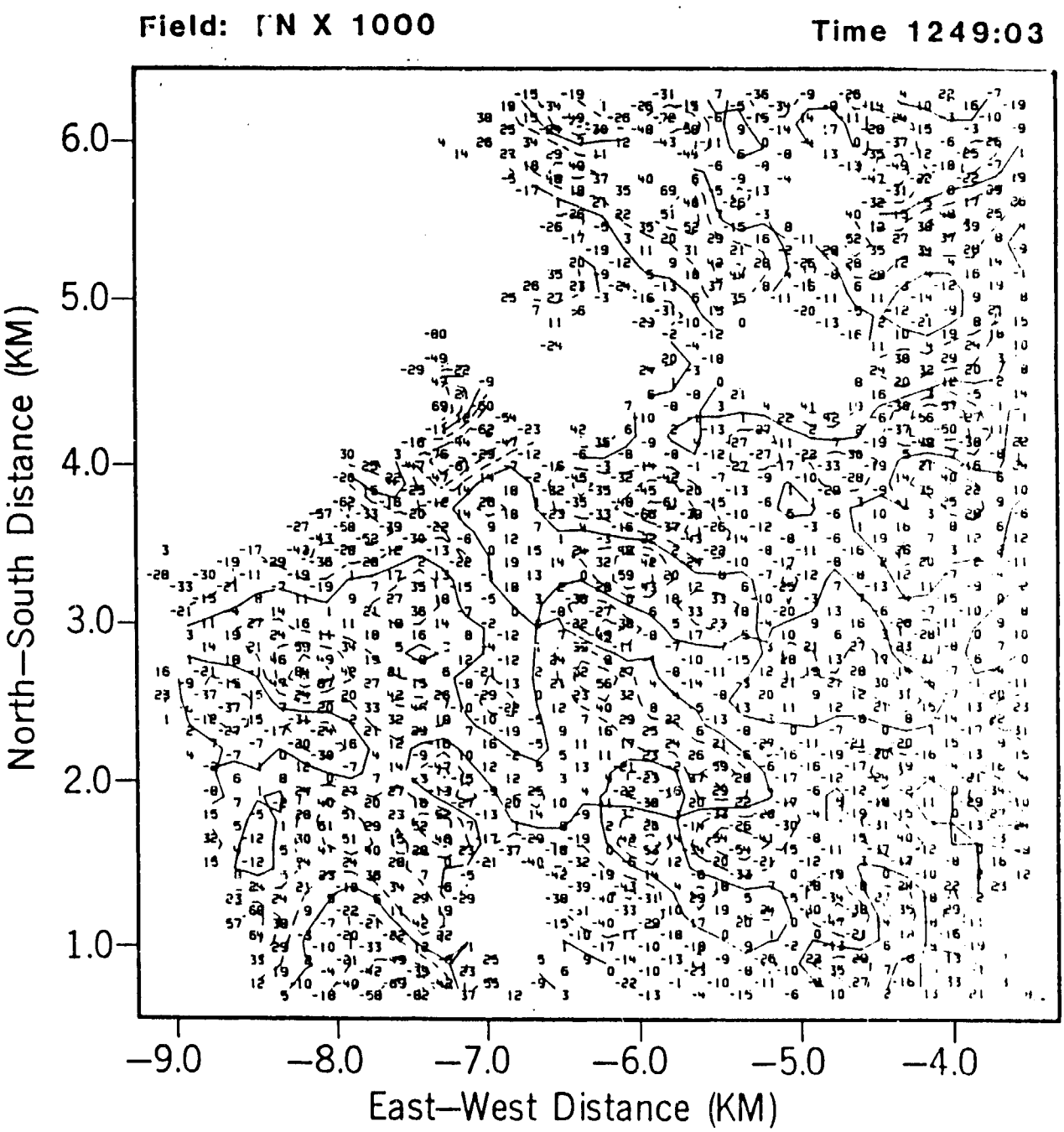
Field: TN X 1000
Time 1249:03
6.0
5.0
4.0
3.0
2.0
1.0
North–South Distance (KM)
–9.0
–8.0
–7.0
–6.0
–5.0
–4.0
East–West Distance (KM)

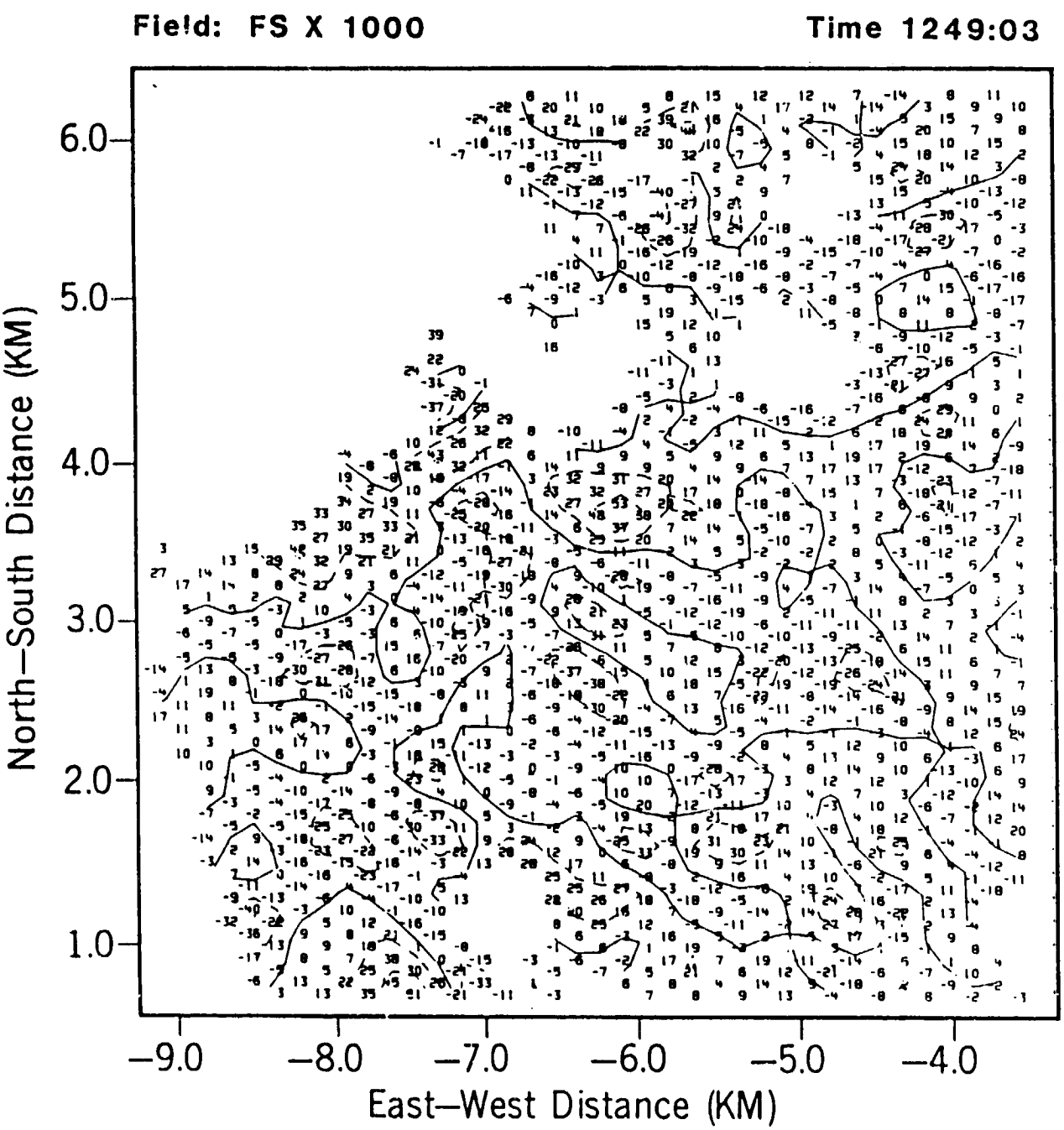
Field: FS X 1000
Time 1249:03
North–South Distance (KM)
6.0
5.0
4.0
3.0
2.0
1.0
–9.0
–8.0
–7.0
–6.0
–5.0
–4.0
East–West Distance (KM)

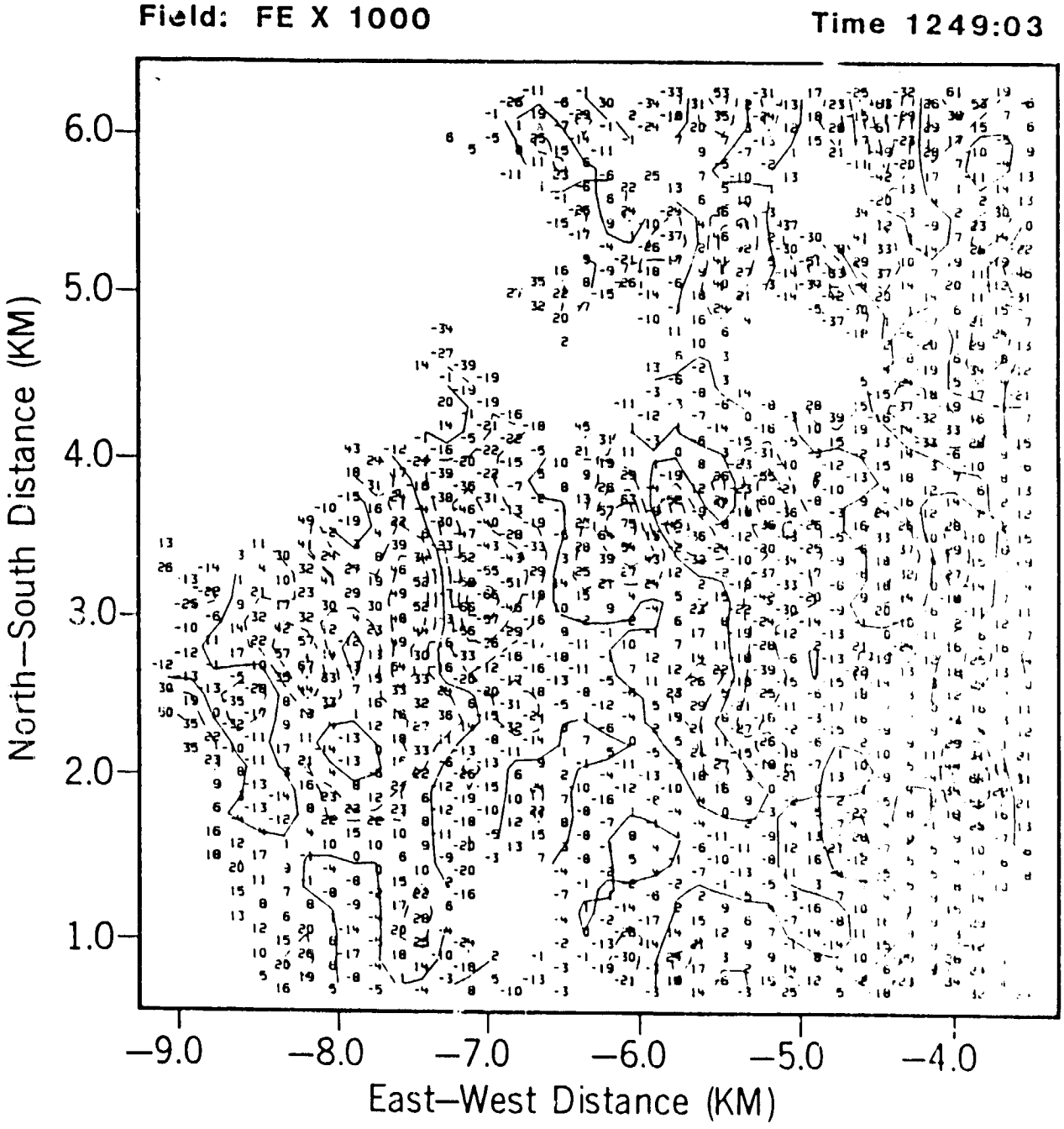

Reproduced from
best available copy.

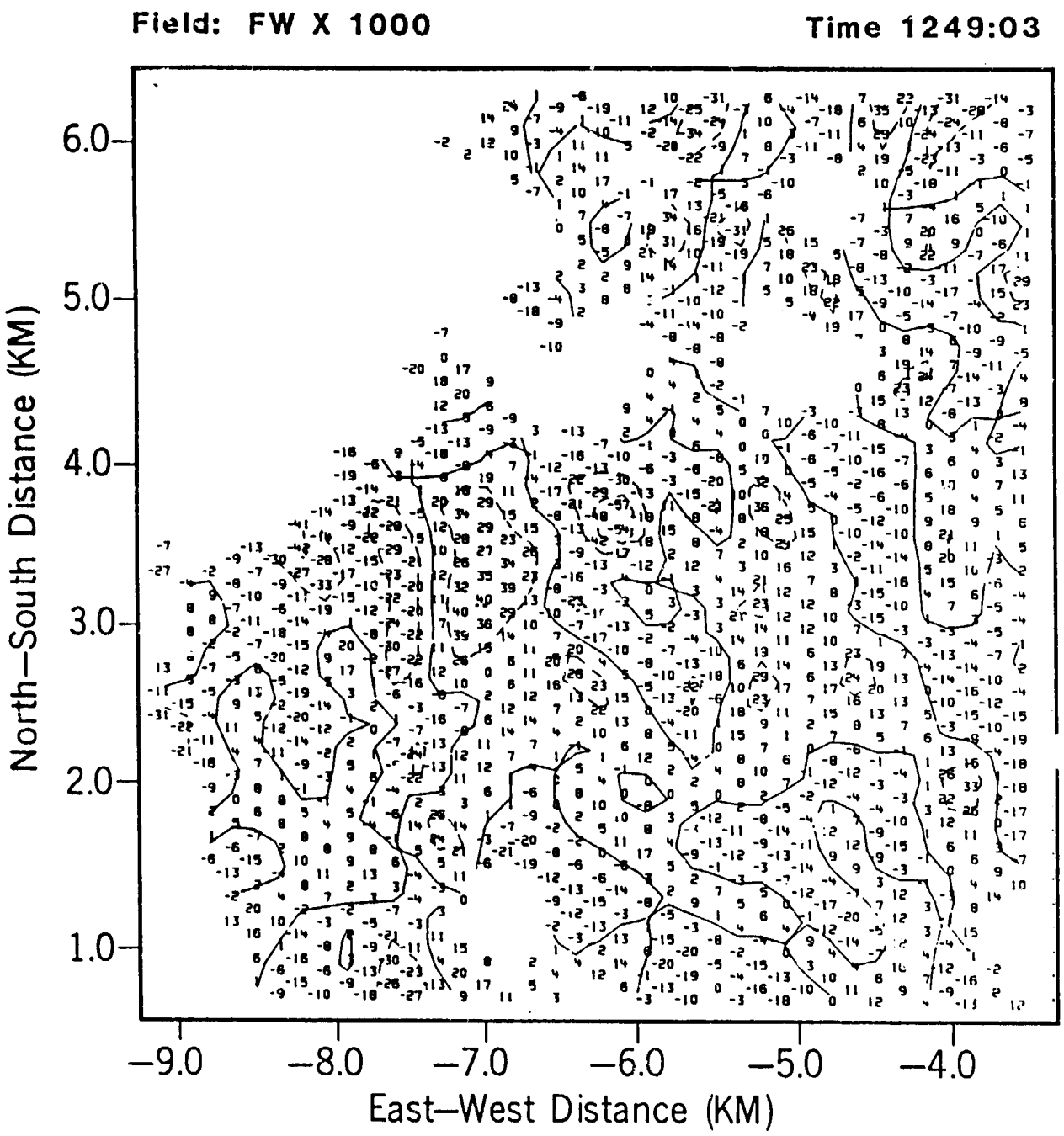
Field: FW X 1000
Time 1249:03
North–South Distance (KM)
6.0
5.0
4.0
3.0
2.0
1.0
−9.0
−8.0
−7.0
−6.0
−5.0
−4.0
East–West Distance (KM)

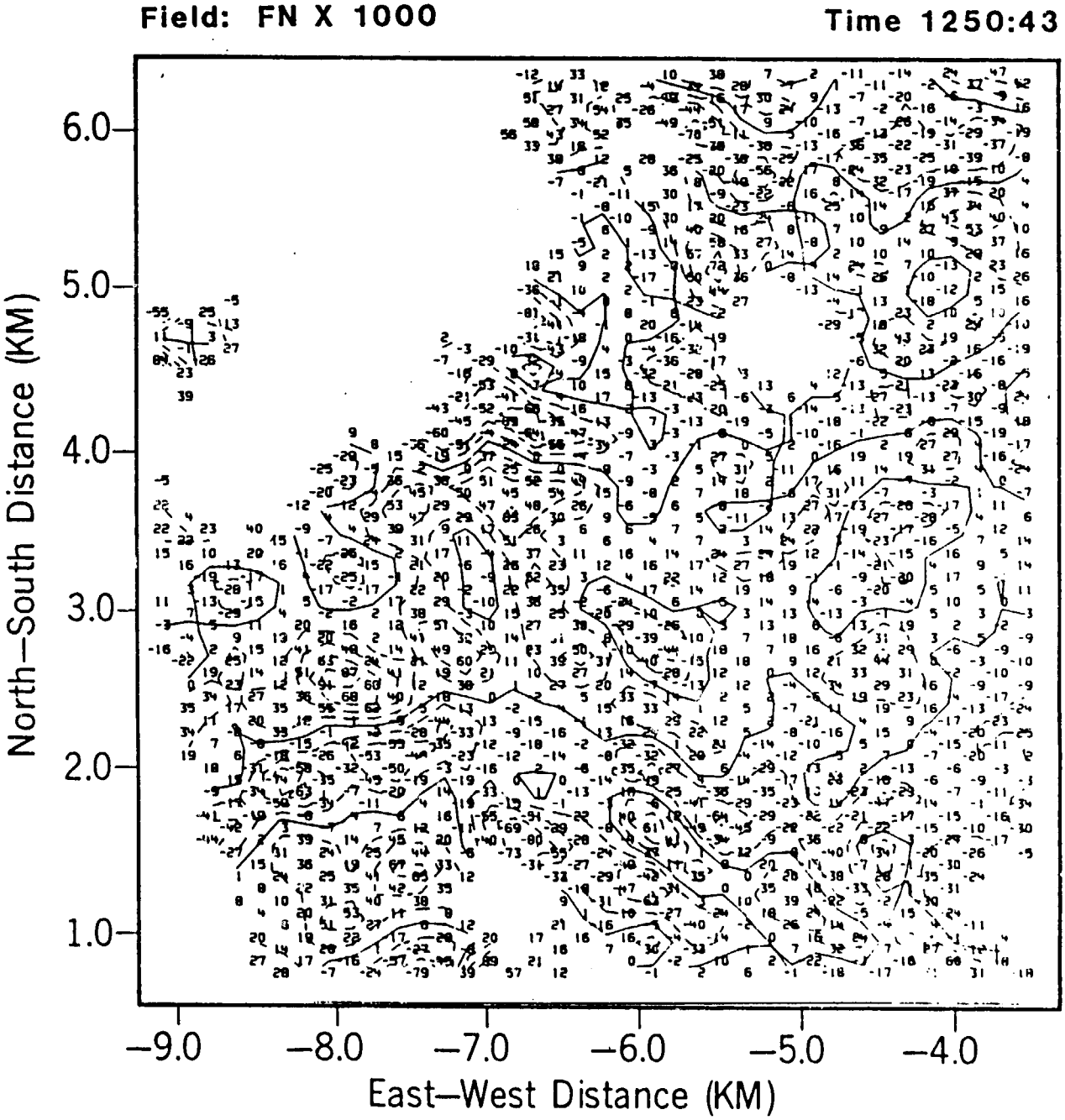
Field: FN X 1000
Time 1250:43
North—South Distance (KM)
6.0
5.0
4.0
3.0
2.0
1.0
−9.0
−8.0
−7.0
−6.0
−5.0
−4.0
East—West Distance (KM)

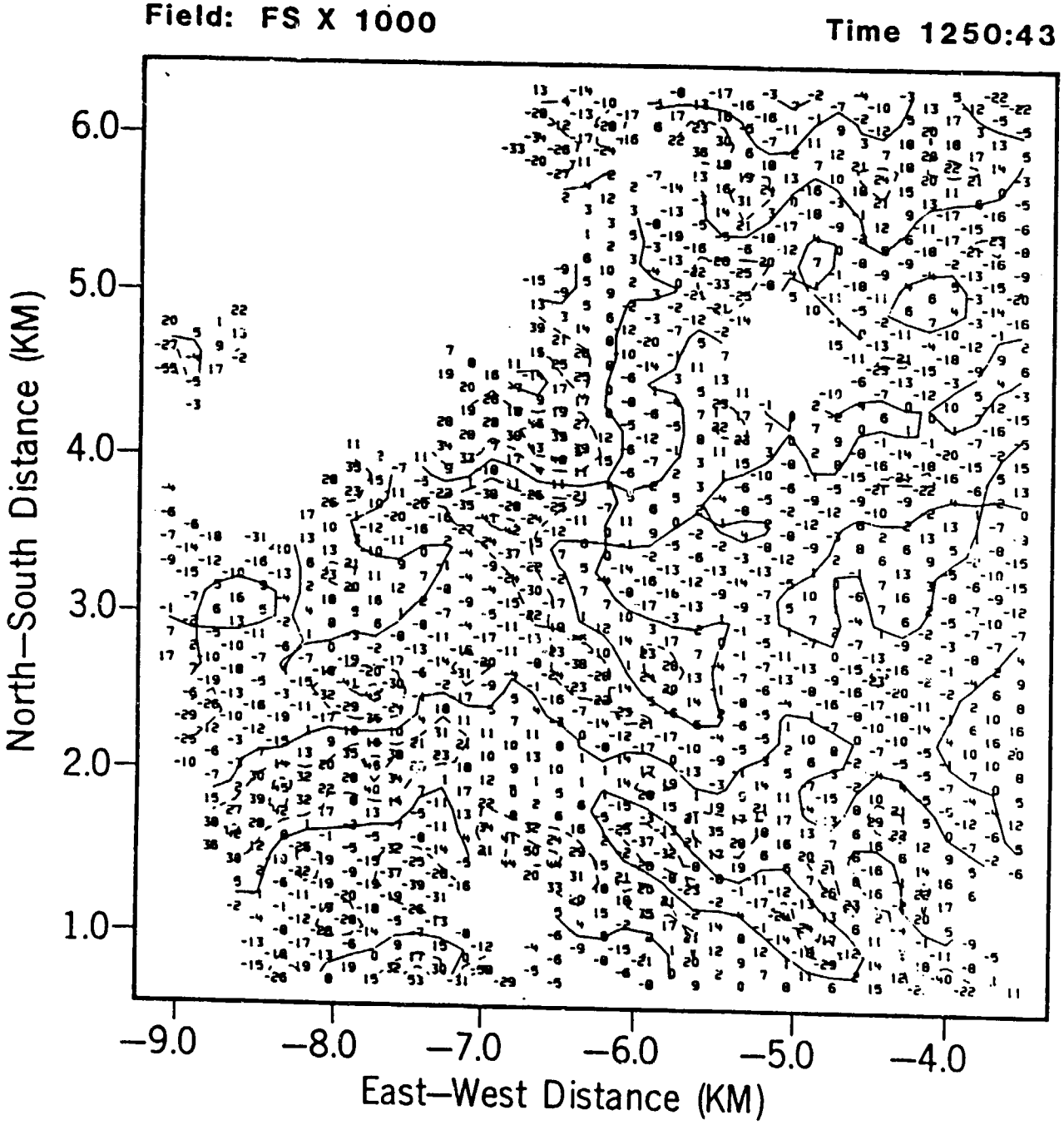
Field: FS X 1000
Time 1250:43
North–South Distance (KM)
6.0
5.0
4.0
3.0
2.0
1.0
–9.0
–8.0
–7.0
–6.0
–5.0
–4.0
East–West Distance (KM)

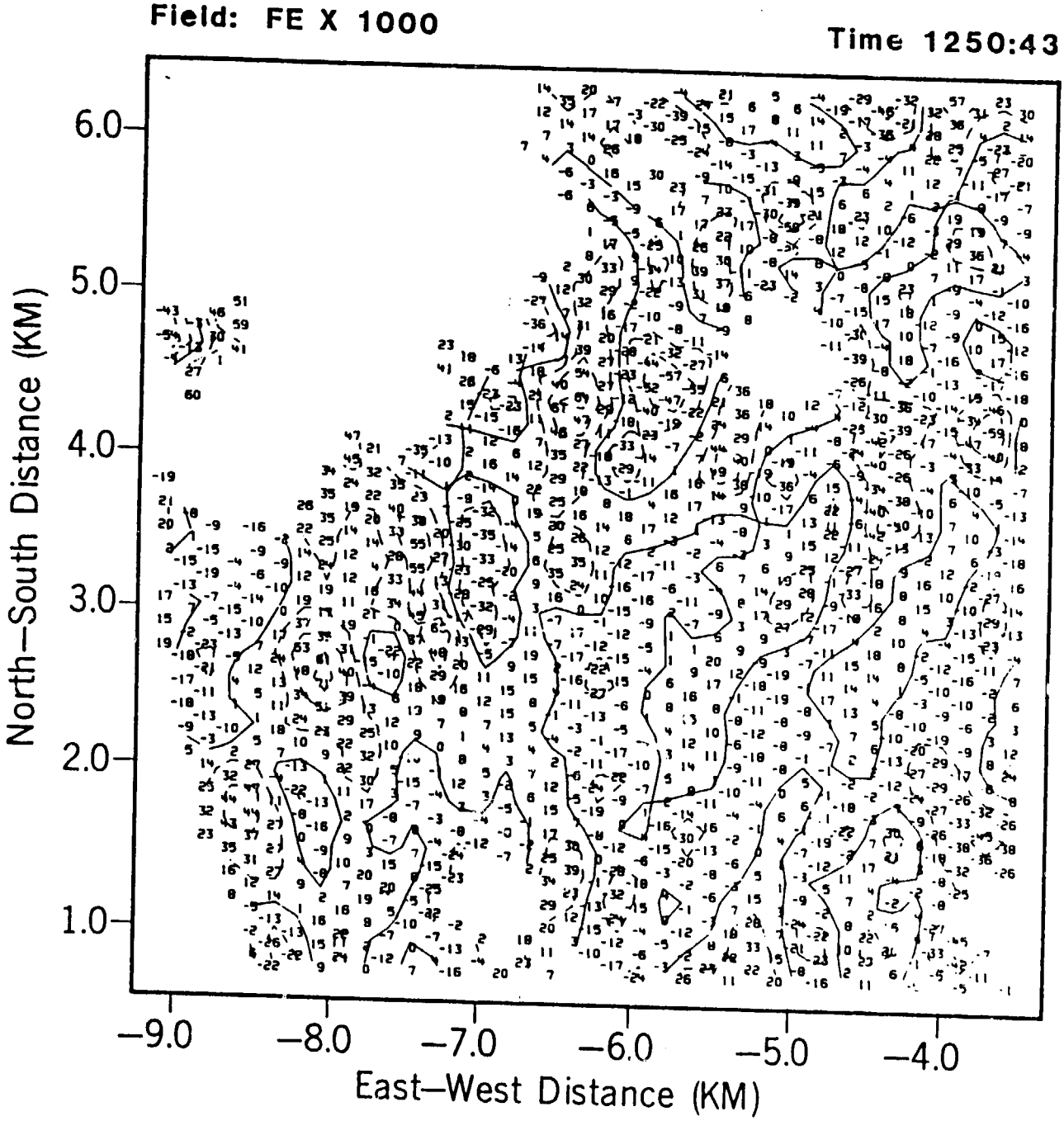
Field: FE X 1000
Time 1250:43
6.0
5.0
4.0
3.0
2.0
1.0
North–South Distance (KM)
–9.0
–8.0
–7.0
–6.0
–5.0
–4.0
East–West Distance (KM)

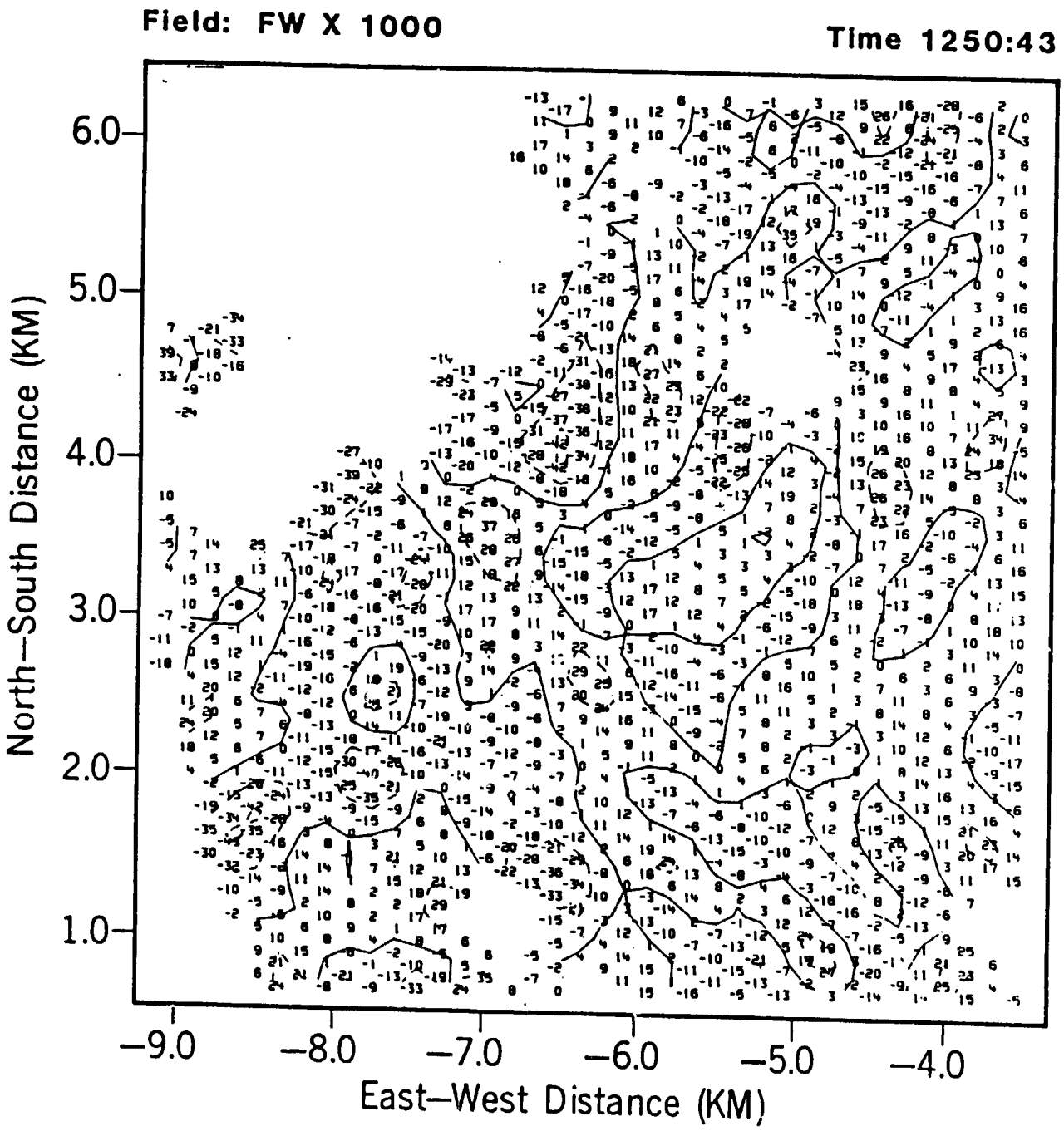
Field: FW X 1000
Time 1250:43
6.0
5.0
4.0
3.0
2.0
1.0
North–South Distance (KM)
–9.0
–8.0
–7.0
–6.0
–5.0
–4.0
East–West Distance (KM)

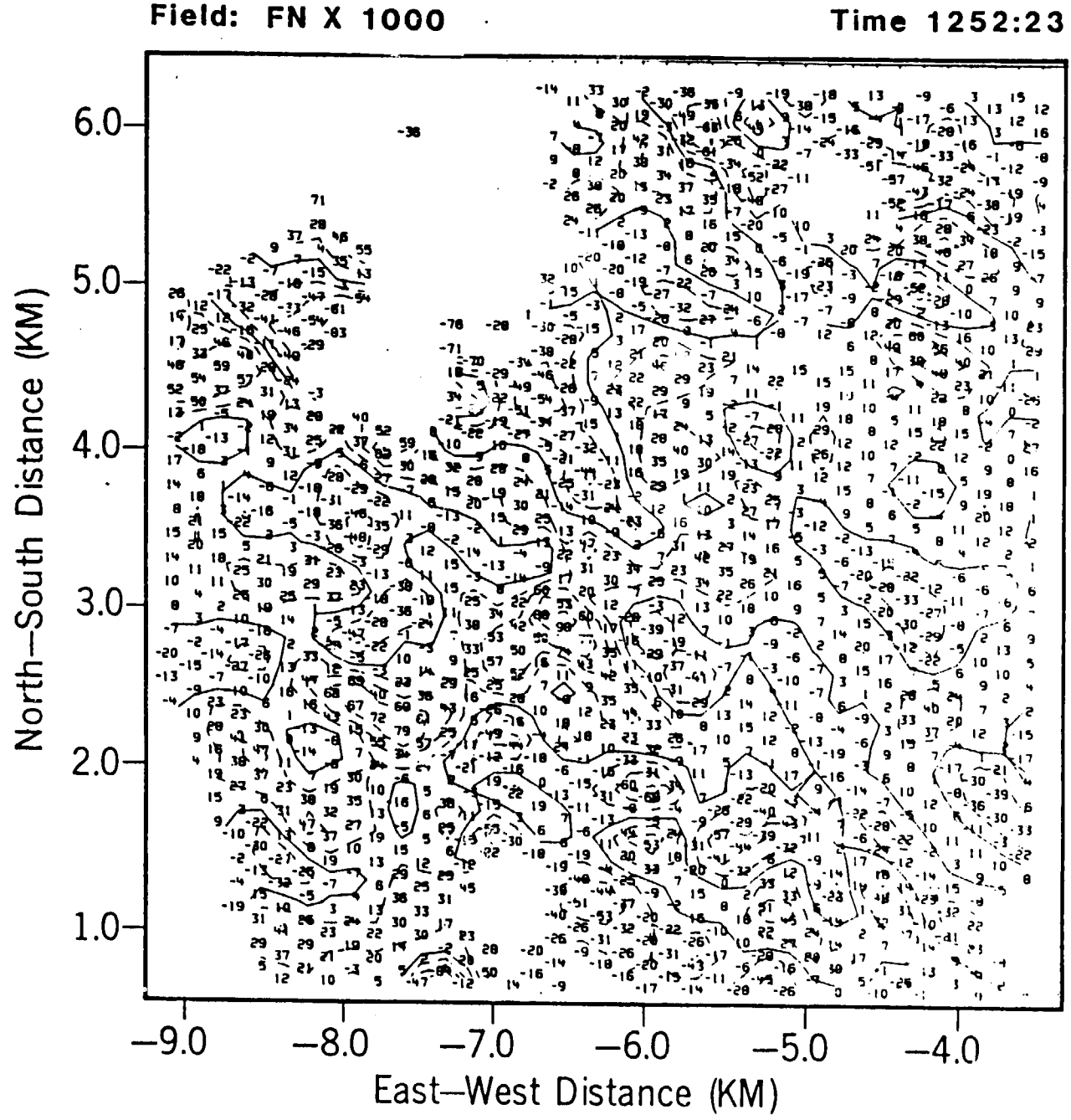
Field: FN X 1000
Time 1252:23
6.0
5.0
4.0
3.0
2.0
1.0
North—South Distance (KM)
-9.0
-8.0
-7.0
-6.0
-5.0
-4.0
East—West Distance (KM)

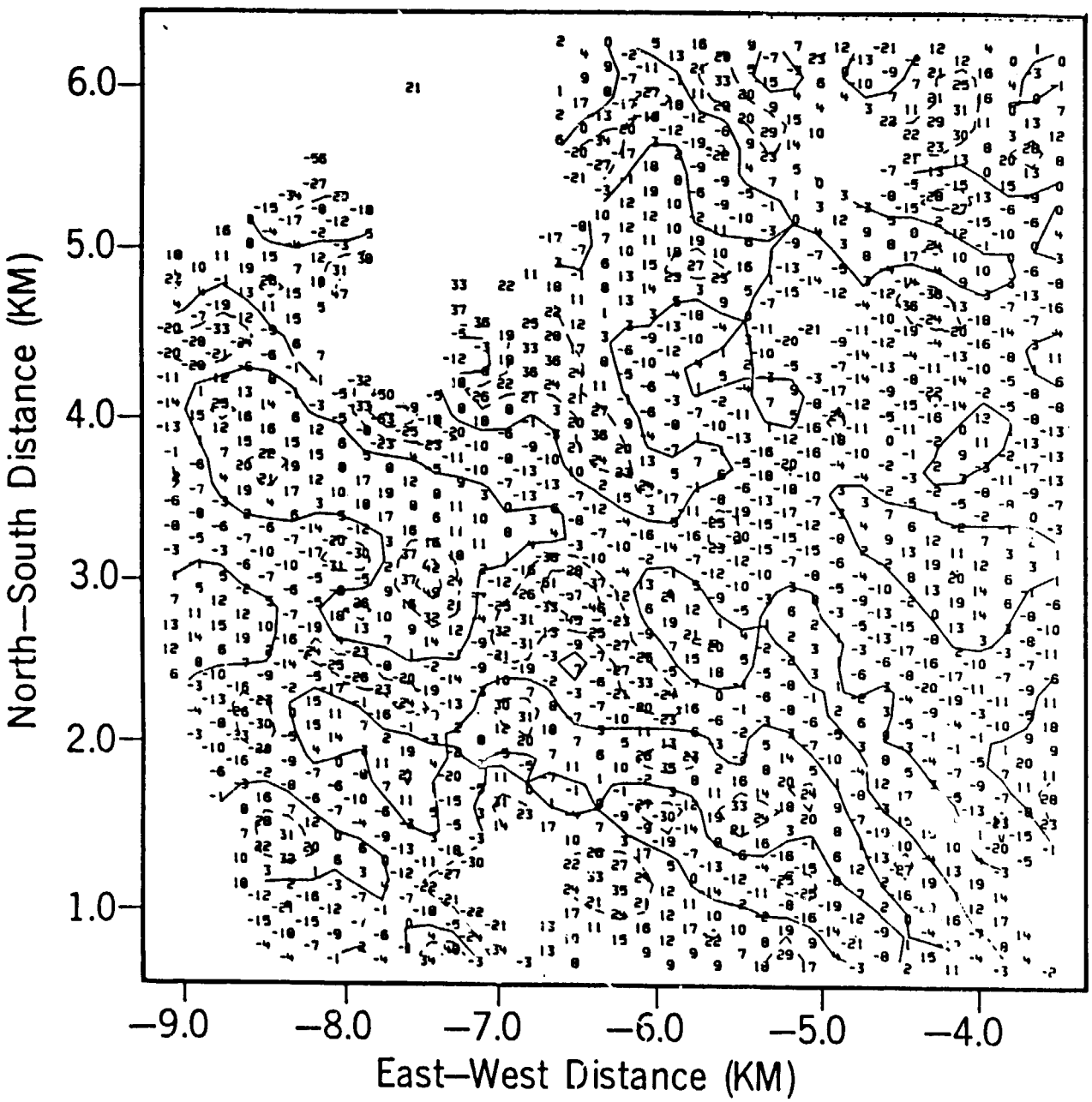
Field: FS X 1000
Time 1252:23
6.0
5.0
4.0
3.0
2.0
1.0
North–South Distance (KM)
–9.0
–8.0
–7.0
–6.0
–5.0
–4.0
East–West Distance (KM)

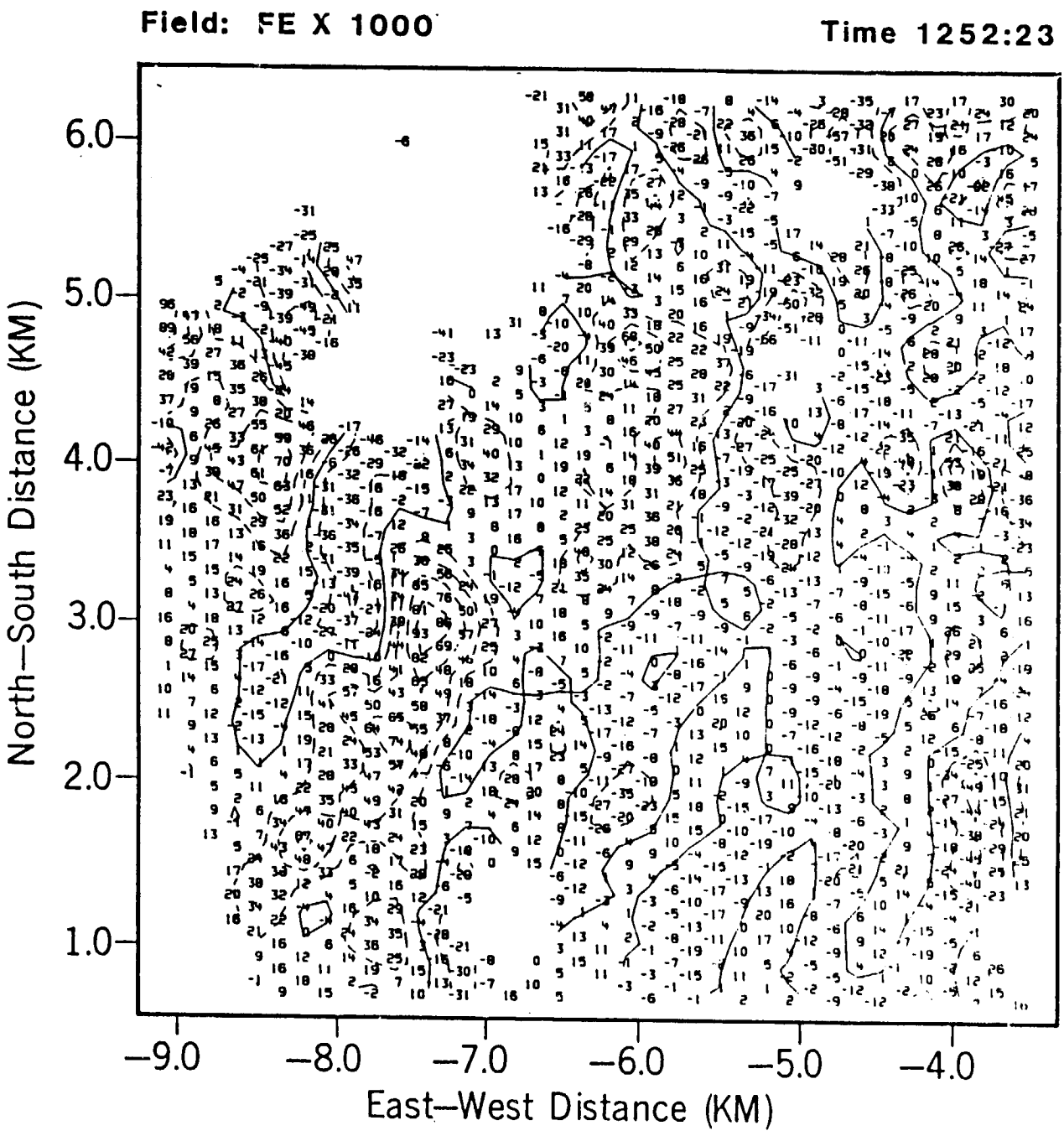
Field: FE X 1000
Time 1252:23
6.0
5.0
4.0
3.0
2.0
1.0
North—South Distance (KM)
−9.0
−8.0
−7.0
−6.0
−5.0
−4.0
East—West Distance (KM)

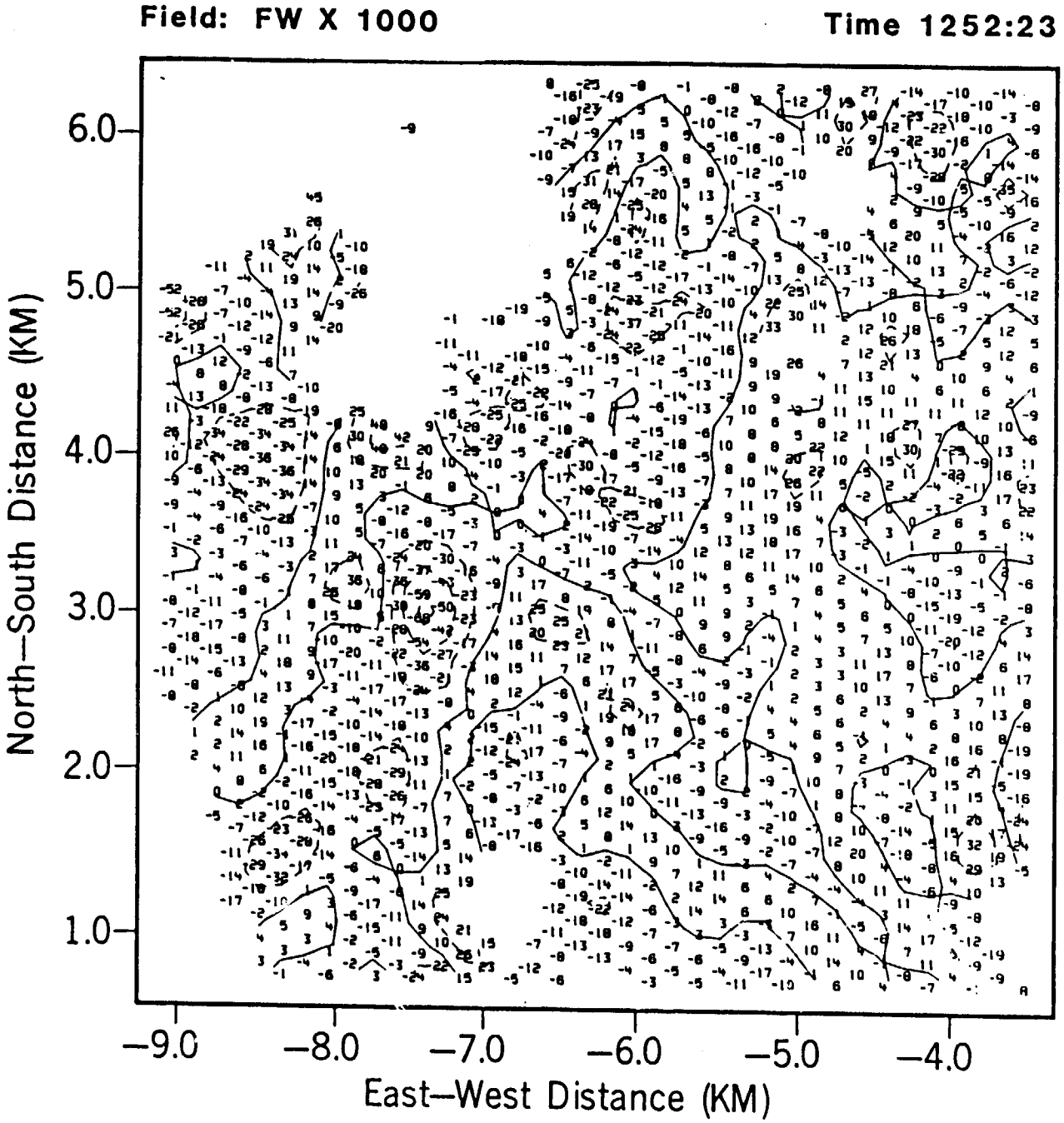
Field: FW X 1000
Time 1252:23
North—South Distance (KM)
6.0
5.0
4.0
3.0
2.0
1.0
−9.0
−8.0
−7.0
−6.0
−5.0
−4.0
East—West Distance (KM)

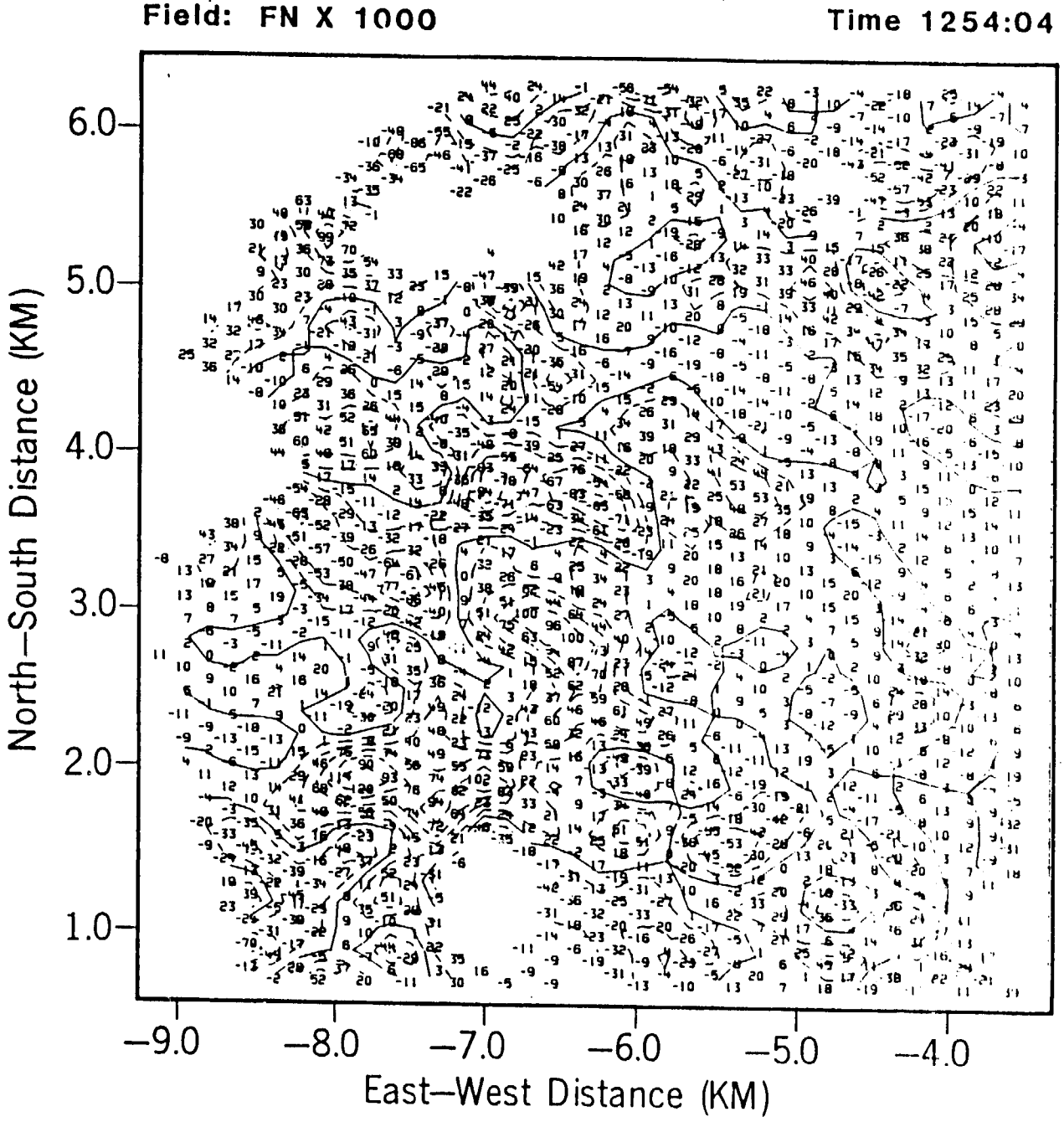
Field: FN X 1000
Time 1254:04
6.0
5.0
4.0
3.0
2.0
1.0
North—South Distance (KM)
—9.0
—8.0
—7.0
—6.0
—5.0
—4.0
East—West Distance (KM)

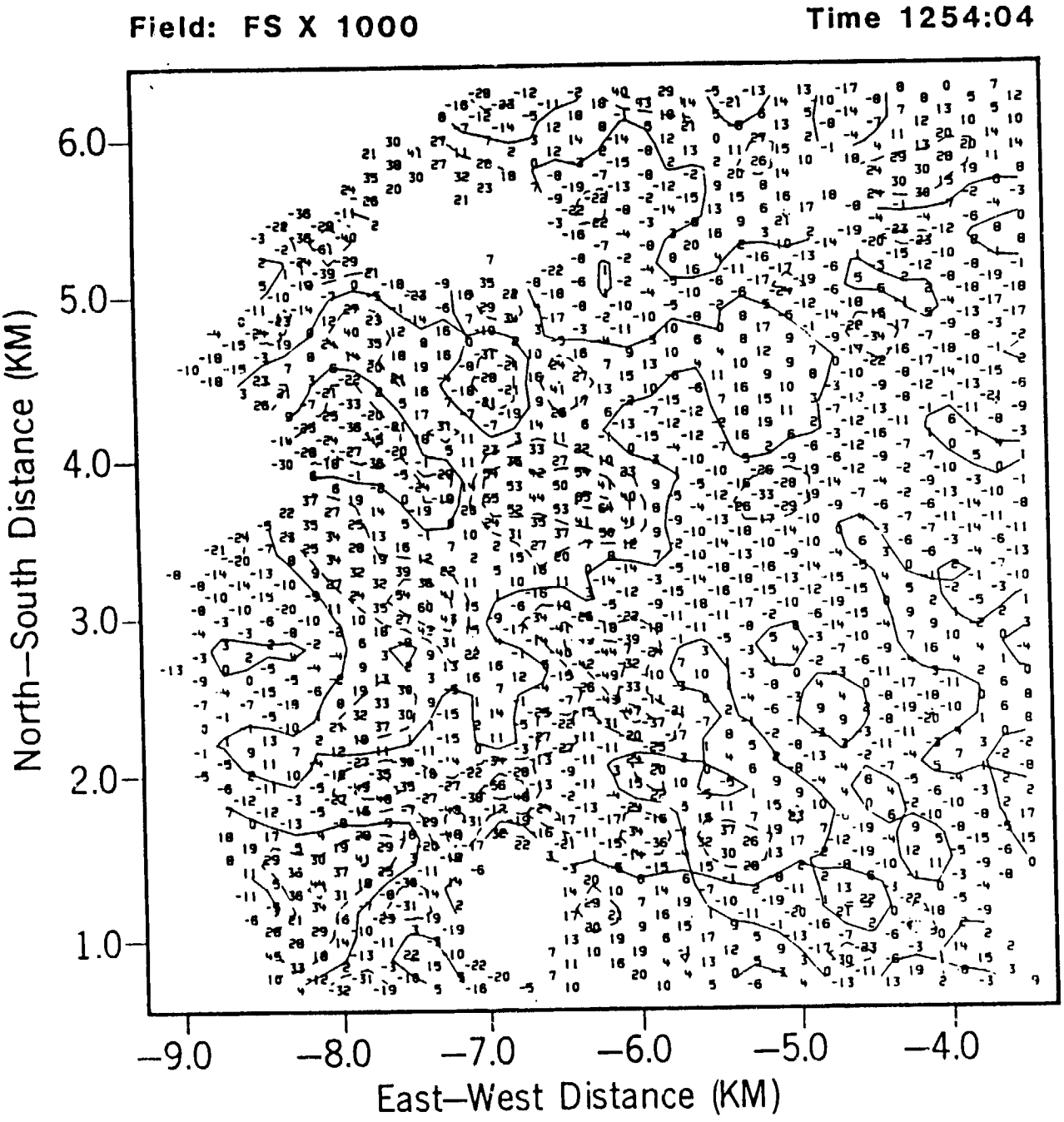
Field: FS X 1000
Time 1254:04
North—South Distance (KM)
6.0
5.0
4.0
3.0
2.0
1.0
−9.0
−8.0
−7.0
−6.0
−5.0
−4.0
East—West Distance (KM)

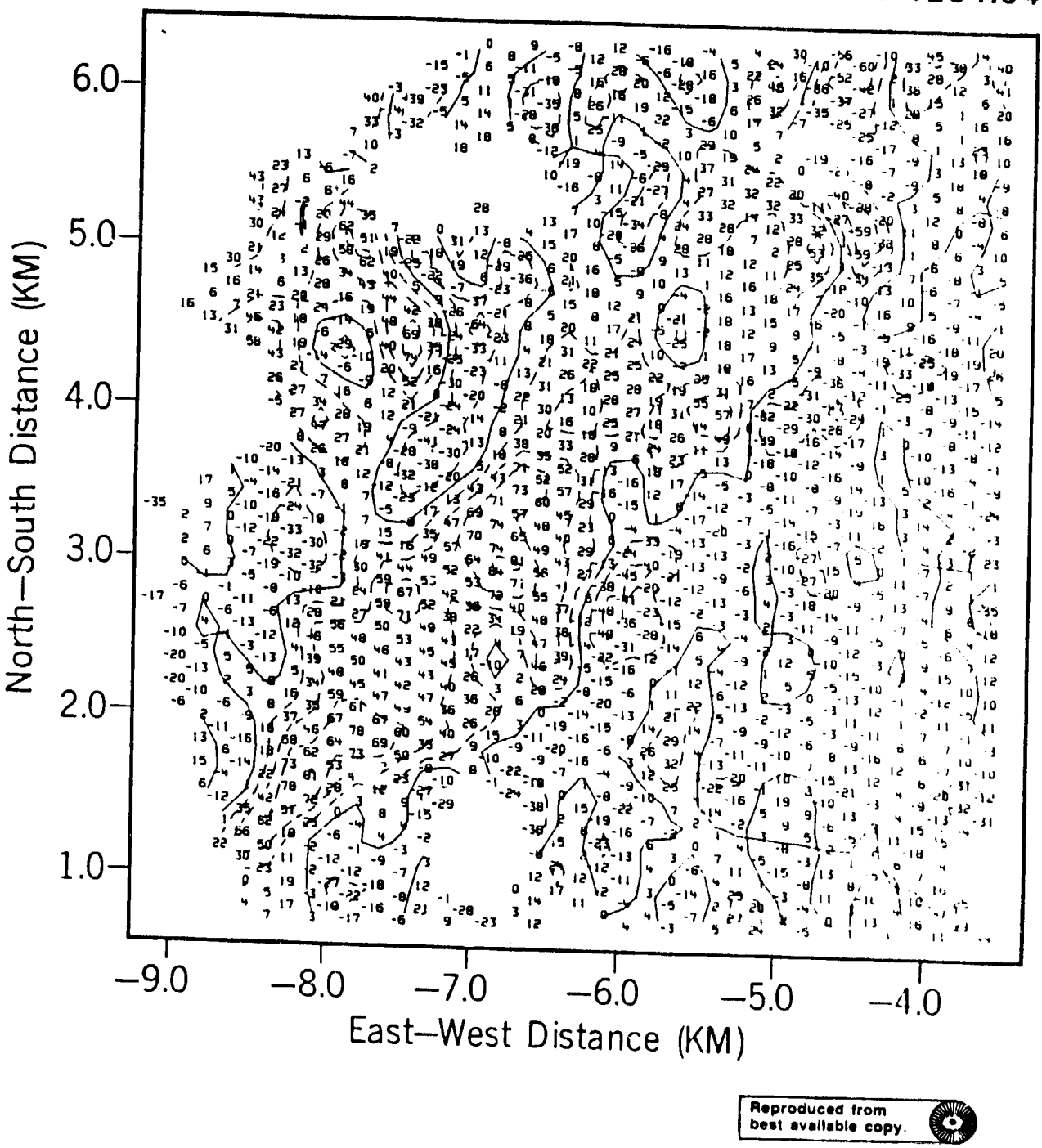

Reproduced from
best available copy.

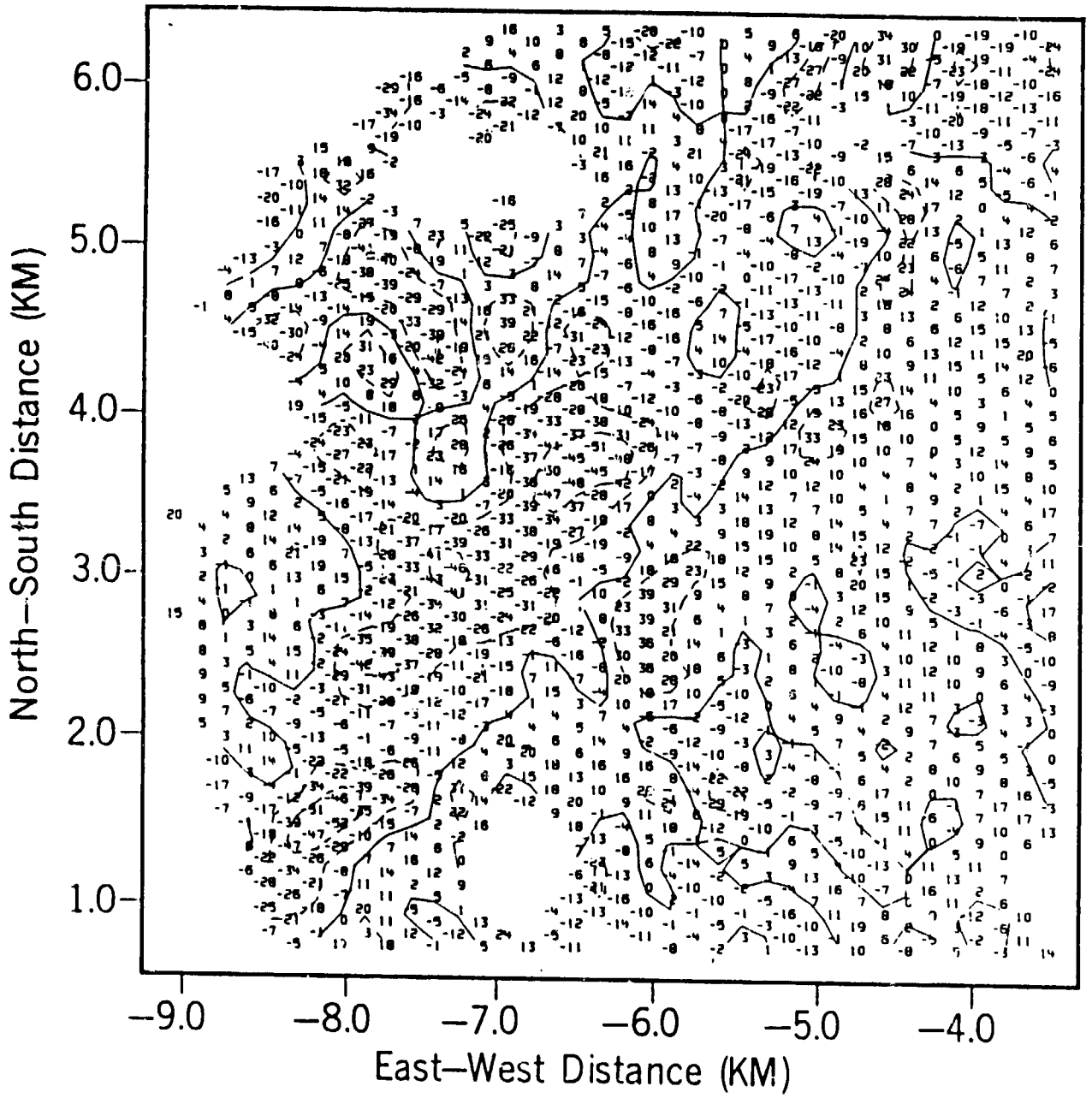
Field: FW X 1000
Time 1254:04
North–South Distance (KM)
6.0
5.0
4.0
3.0
2.0
1.0
–9.0
–8.0
–7.0
–6.0
–5.0
–4.0
East–West Distance (KM)

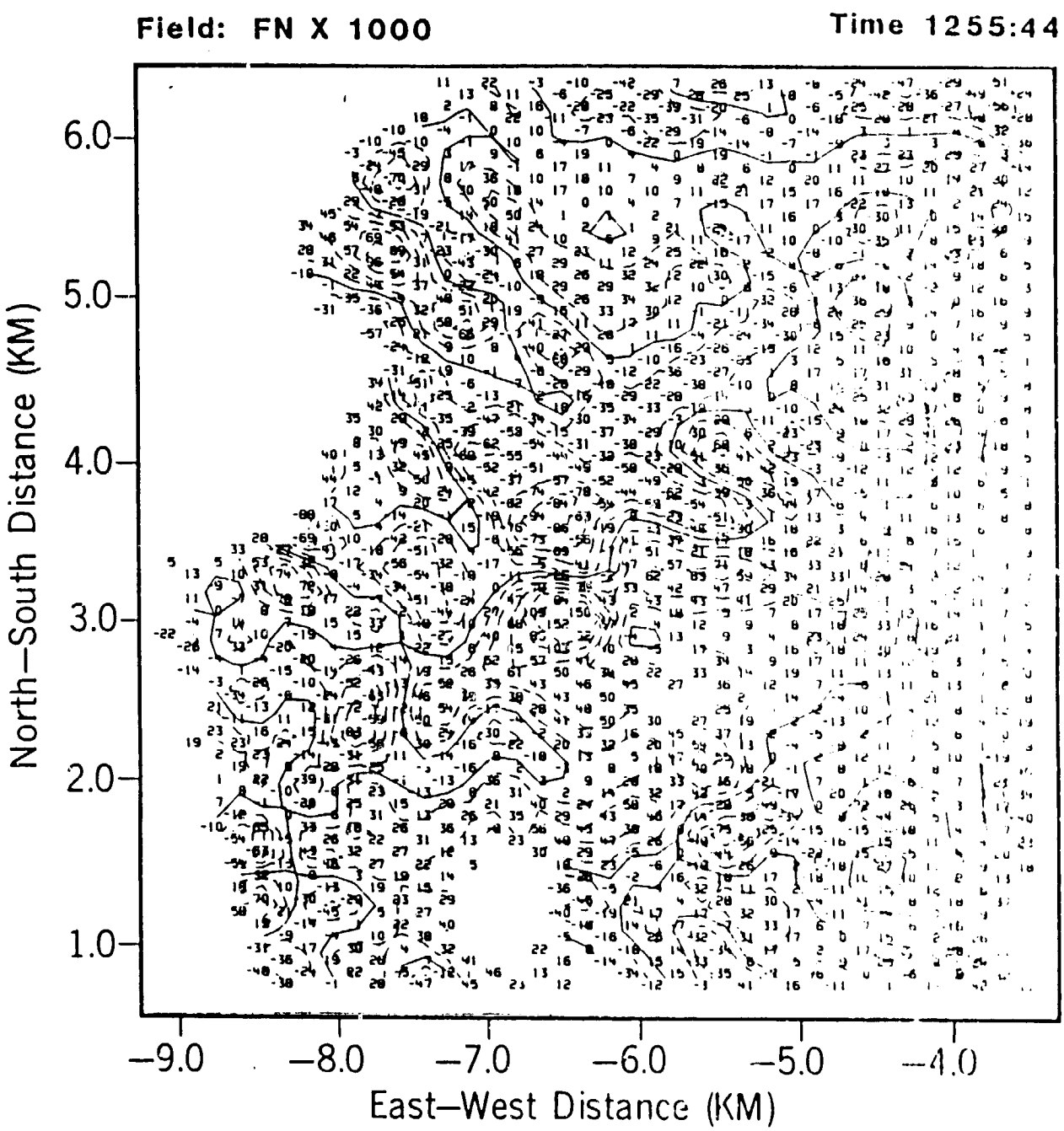
Field: FN X 1000
Time 1255:44
6.0
5.0
4.0
3.0
2.0
1.0
North–South Distance (KM)
–9.0
–8.0
–7.0
–6.0
–5.0
–4.0
East–West Distance (KM)

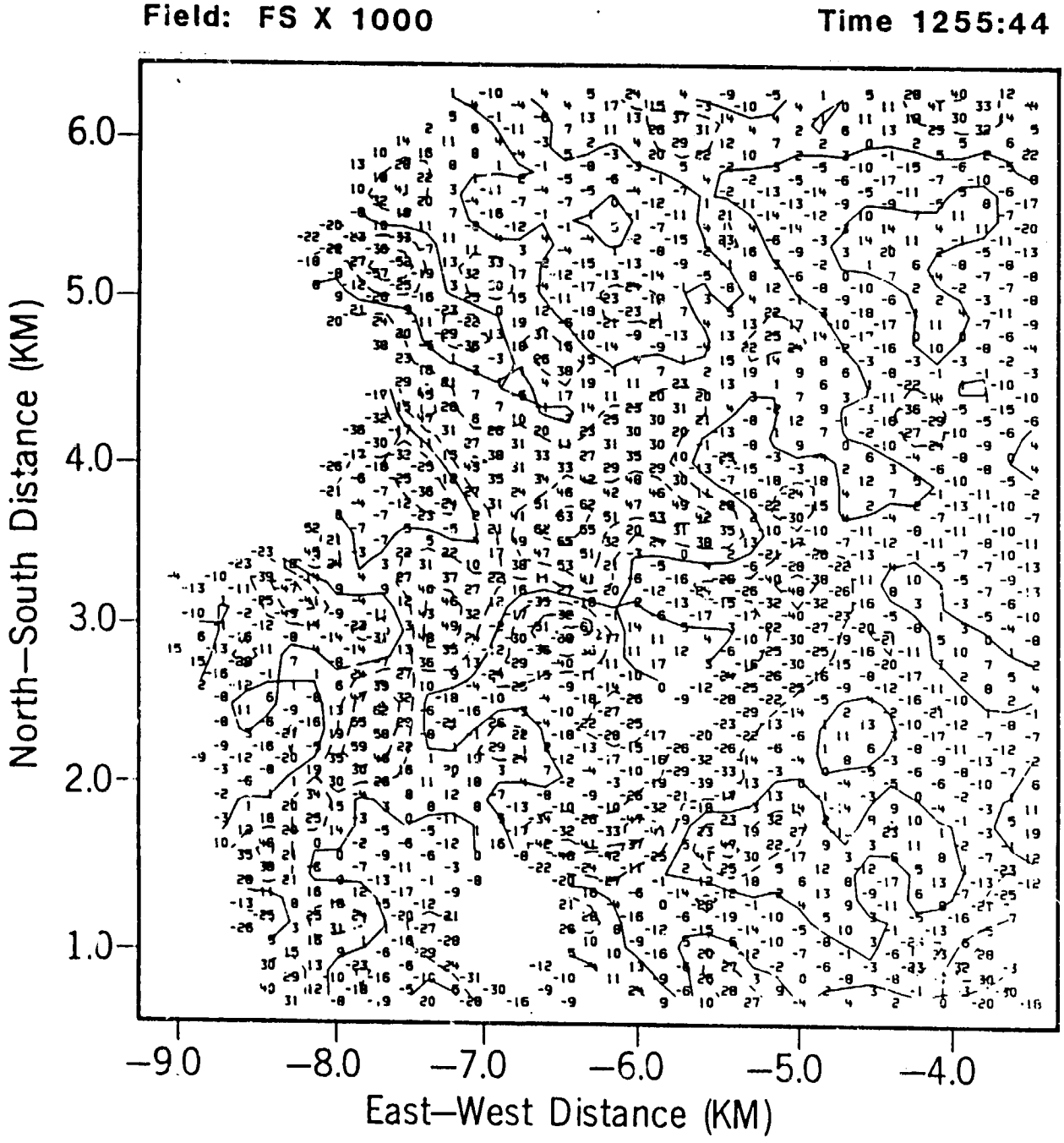
Field: FS X 1000
Time 1255:44
North–South Distance (KM)
6.0
5.0
4.0
3.0
2.0
1.0
–9.0
–8.0
–7.0
–6.0
–5.0
–4.0
East–West Distance (KM)

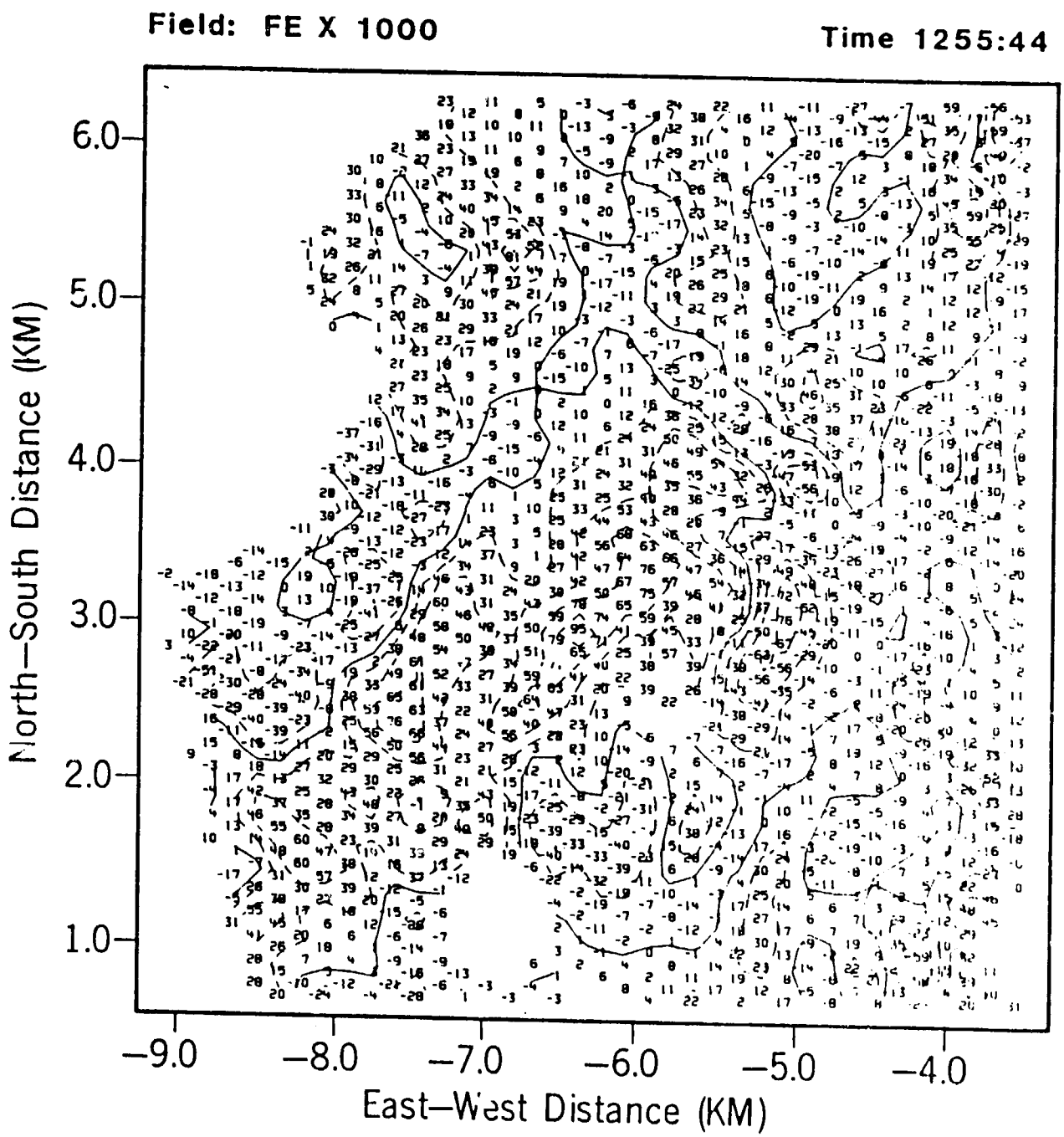
Field: FE X 1000
Time 1255:44
6.0
5.0
4.0
3.0
2.0
1.0
North–South Distance (KM)
–9.0
–8.0
–7.0
–6.0
–5.0
–4.0
East–West Distance (KM)

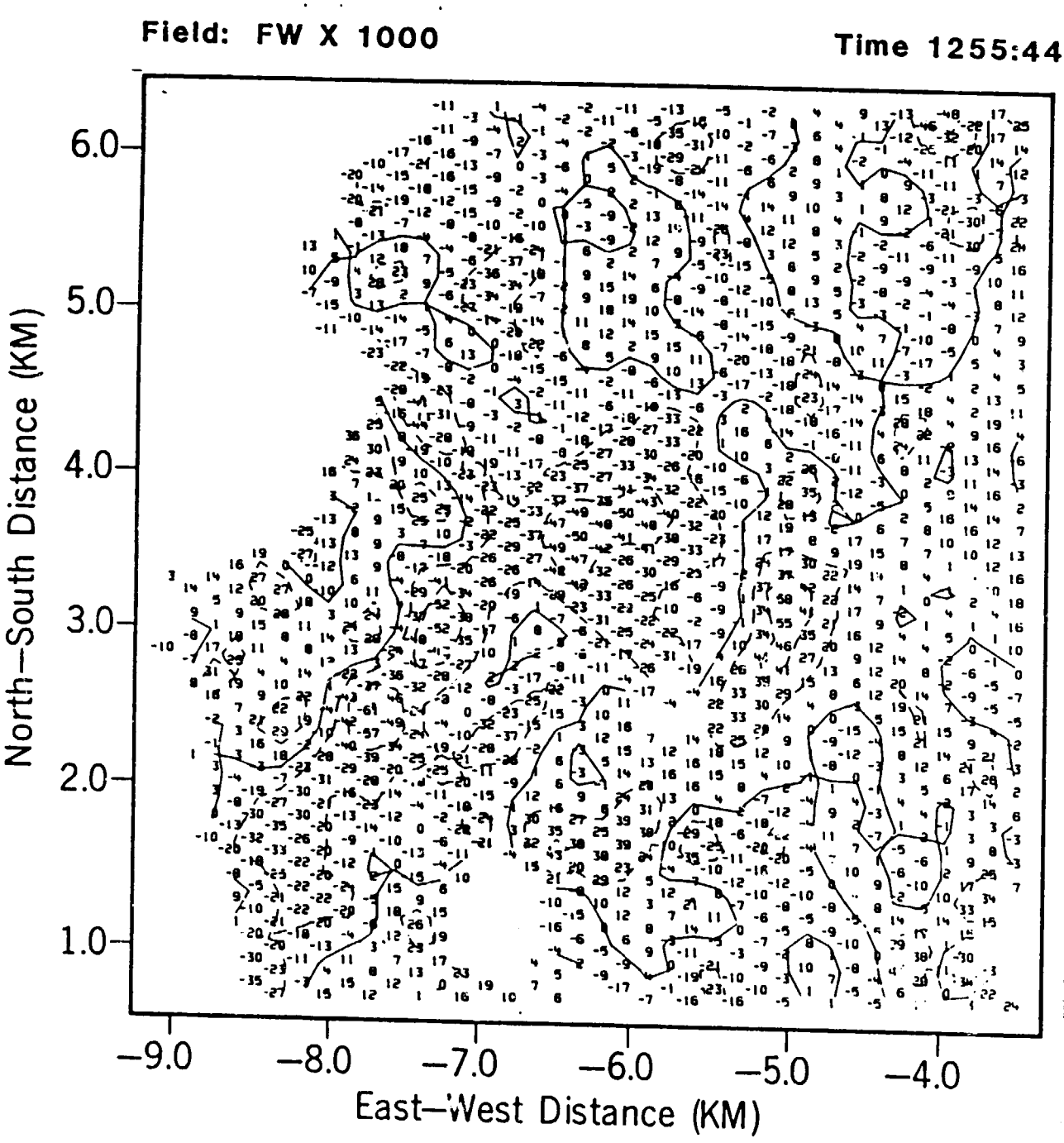
Field: FW X 1000
Time 1255:44
North—South Distance (KM)
6.0
5.0
4.0
3.0
2.0
1.0
−9.0
−8.0
−7.0
−6.0
−5.0
−4.0
East—West Distance (KM)

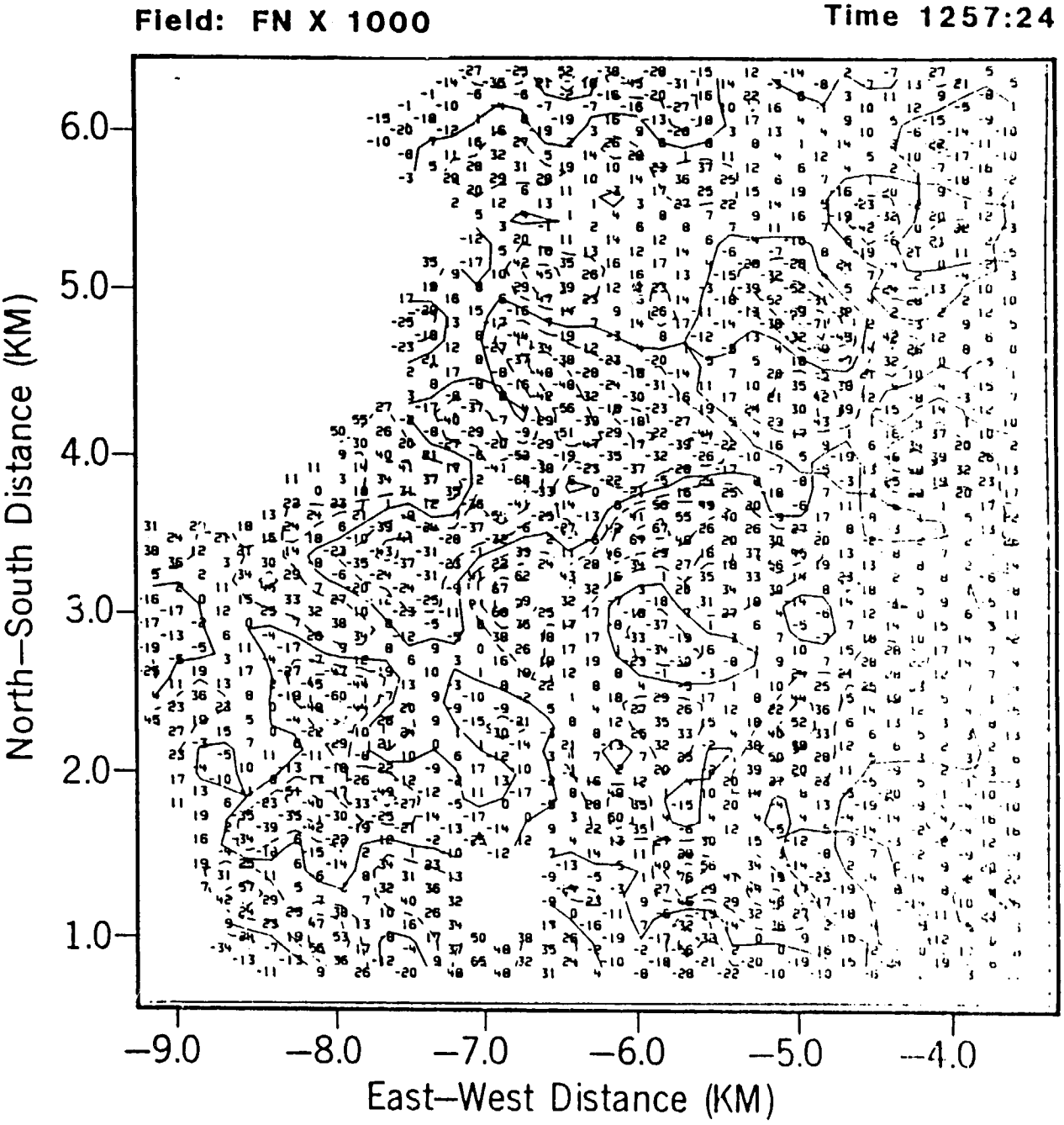
Field: FN X 1000
Time 1257:24
6.0
5.0
4.0
3.0
2.0
1.0
North—South Distance (KM)
—9.0
—8.0
—7.0
—6.0
—5.0
—4.0
East—West Distance (KM)

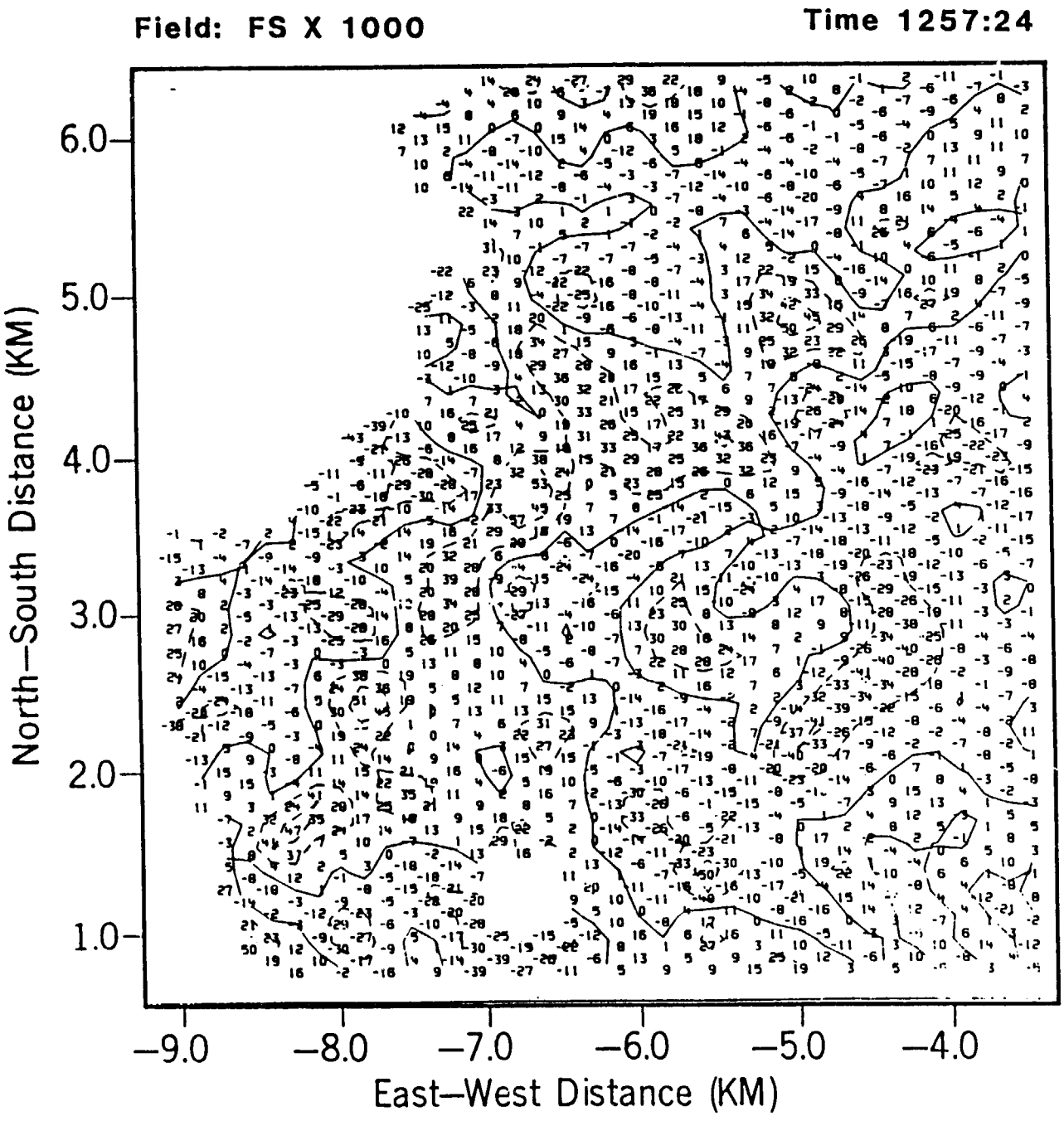
Field: FS X 1000
Time 1257:24
6.0
5.0
4.0
3.0
2.0
1.0
North—South Distance (KM)
-9.0
-8.0
-7.0
-6.0
-5.0
-4.0
East—West Distance (KM)

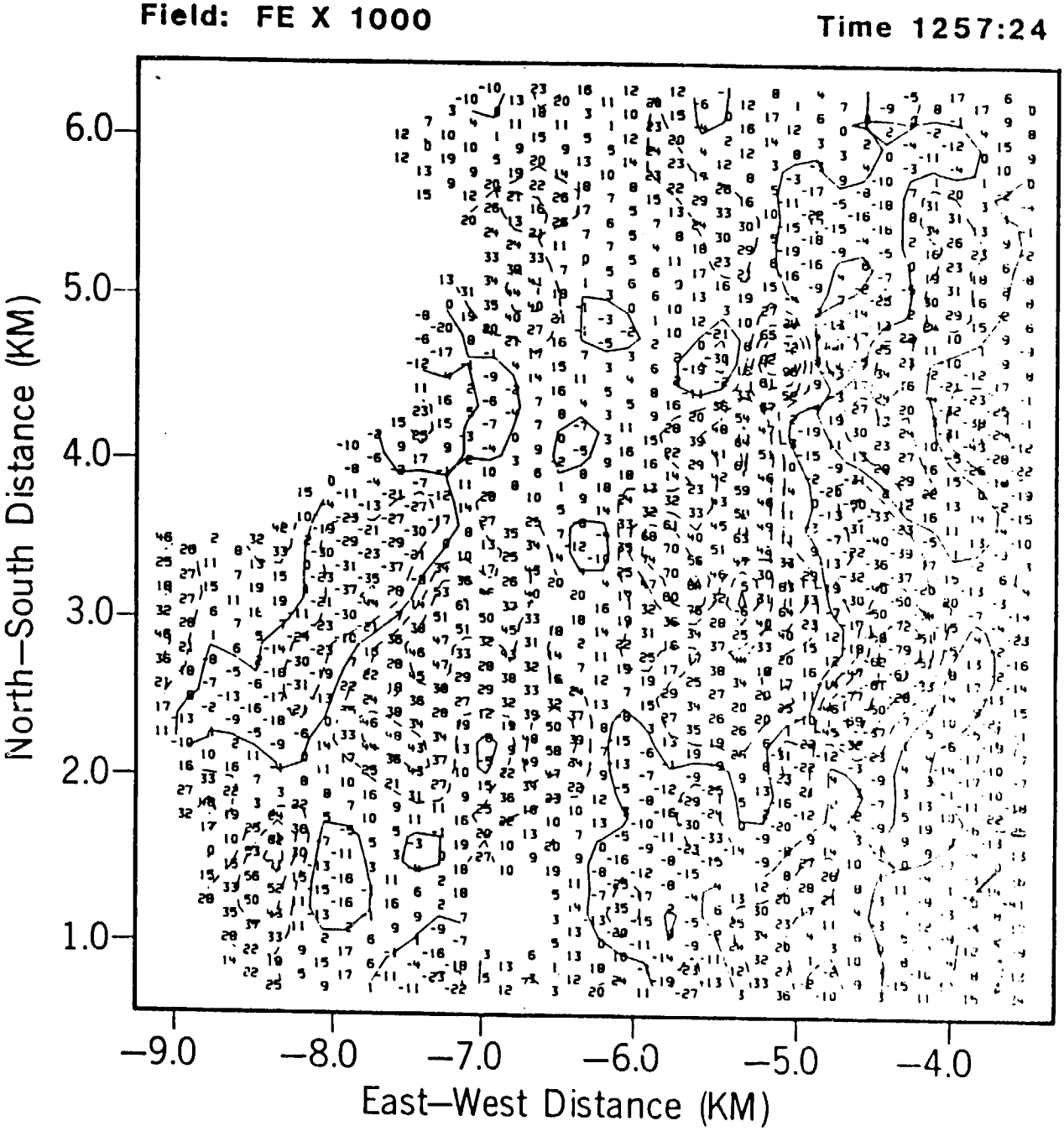
Field: FE X 1000
Time 1257:24
6.0
5.0
4.0
3.0
2.0
1.0
North—South Distance (KM)
—9.0
—8.0
—7.0
—6.0
—5.0
—4.0
East—West Distance (KM)

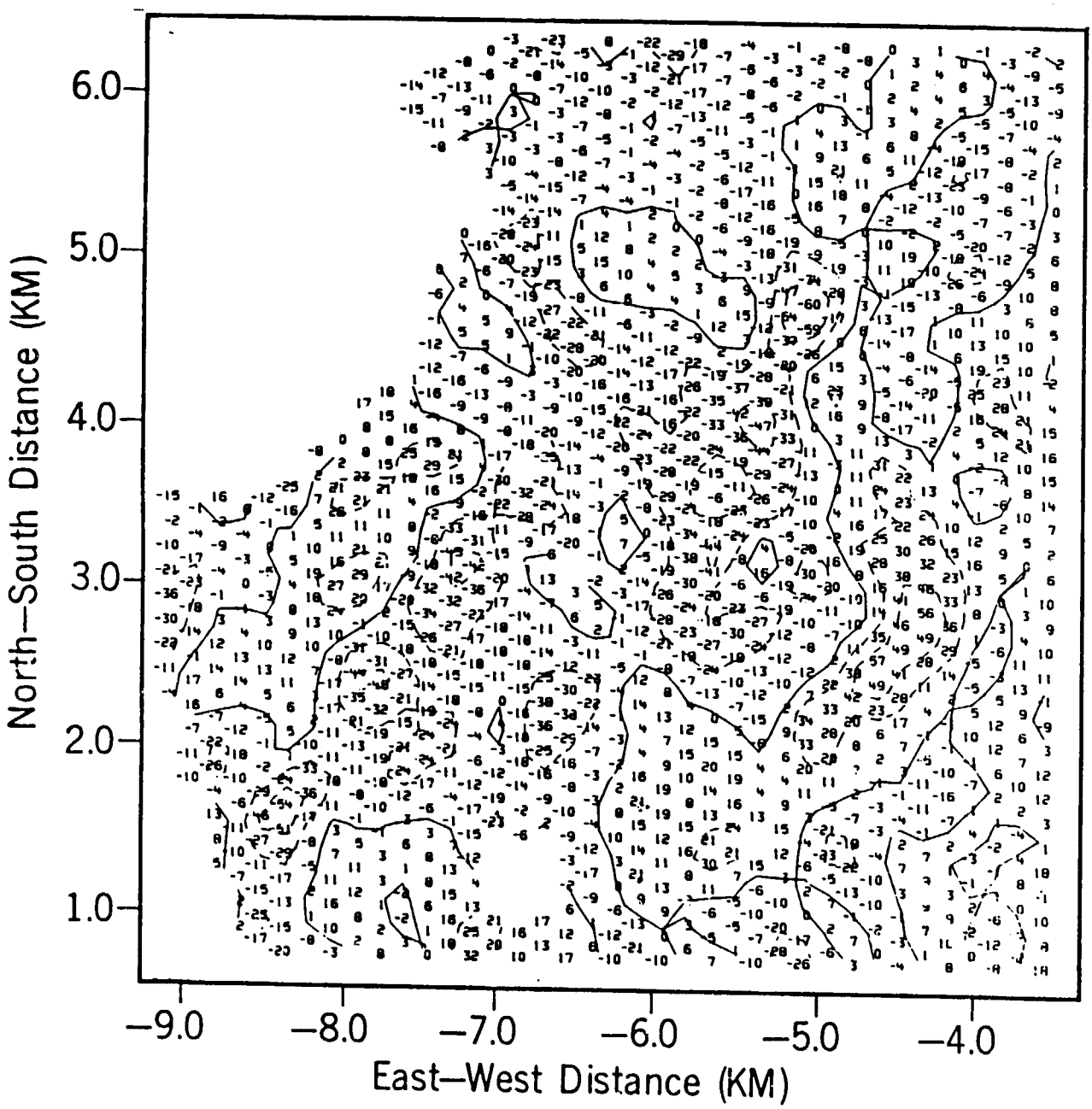
Field: FW X 1000
Time 1257:24
North–South Distance (KM)
6.0
5.0
4.0
3.0
2.0
1.0
–9.0
–8.0
–7.0
–6.0
–5.0
–4.0
East–West Distance (KM)

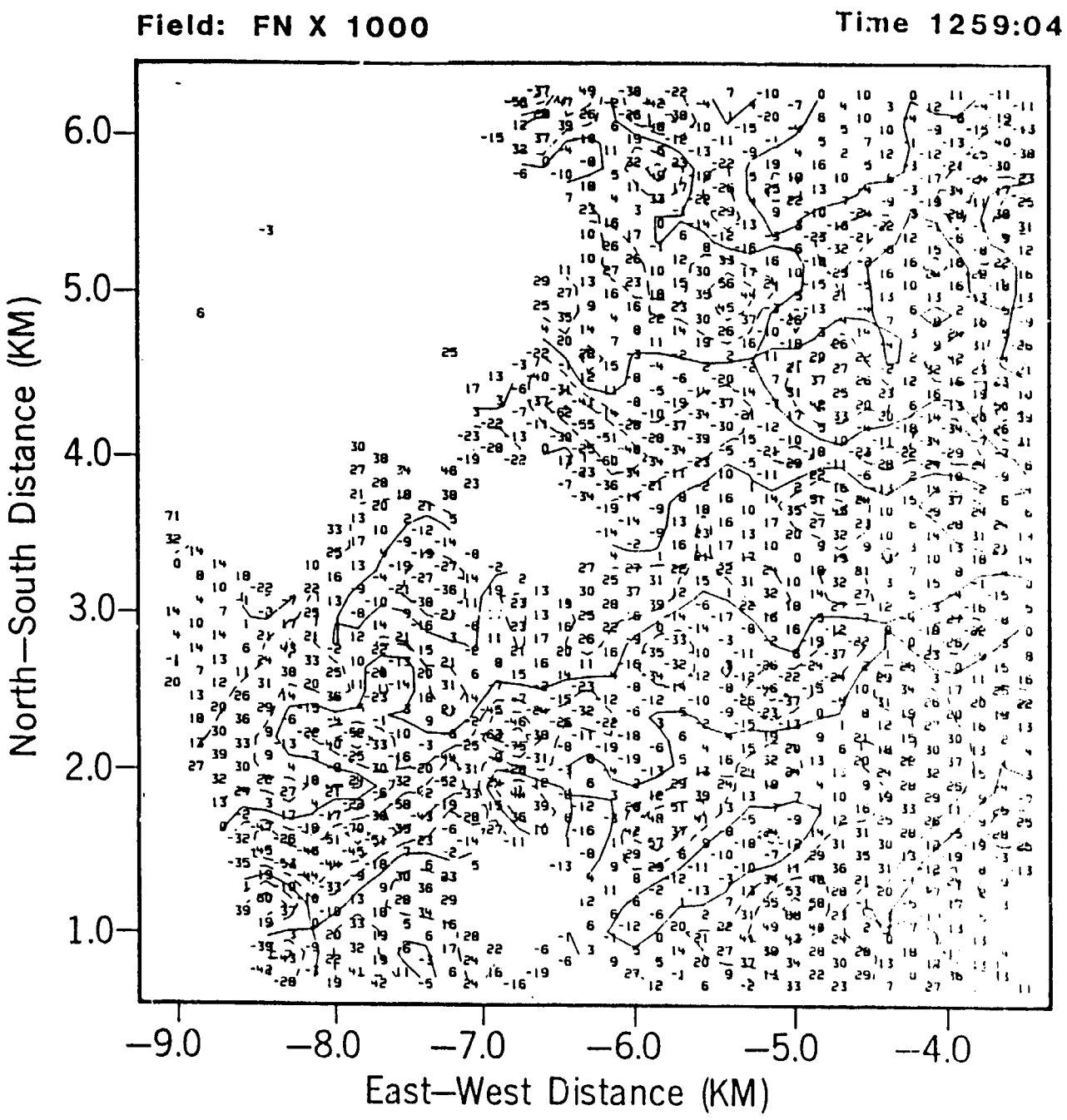
Field: FN X 1000
Time 1259:04
North—South Distance (KM)
6.0
5.0
4.0
3.0
2.0
1.0
—9.0
—8.0
—7.0
—6.0
—5.0
—4.0
East—West Distance (KM)

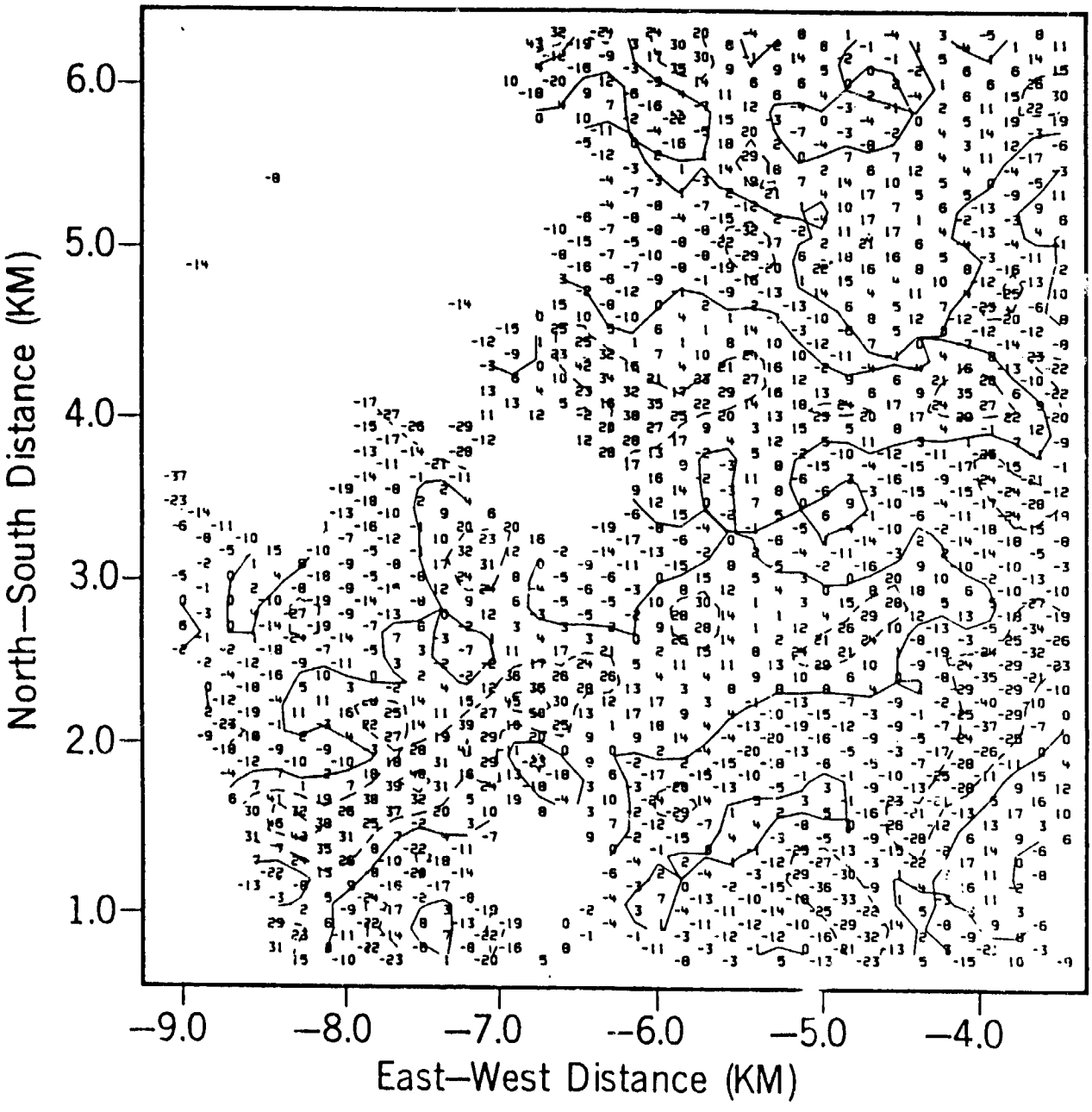
Field: FS X 1000
Time 1259:04
North–South Distance (KM)
6.0
5.0
4.0
3.0
2.0
1.0
–9.0
–8.0
–7.0
–6.0
–5.0
–4.0
East–West Distance (KM)

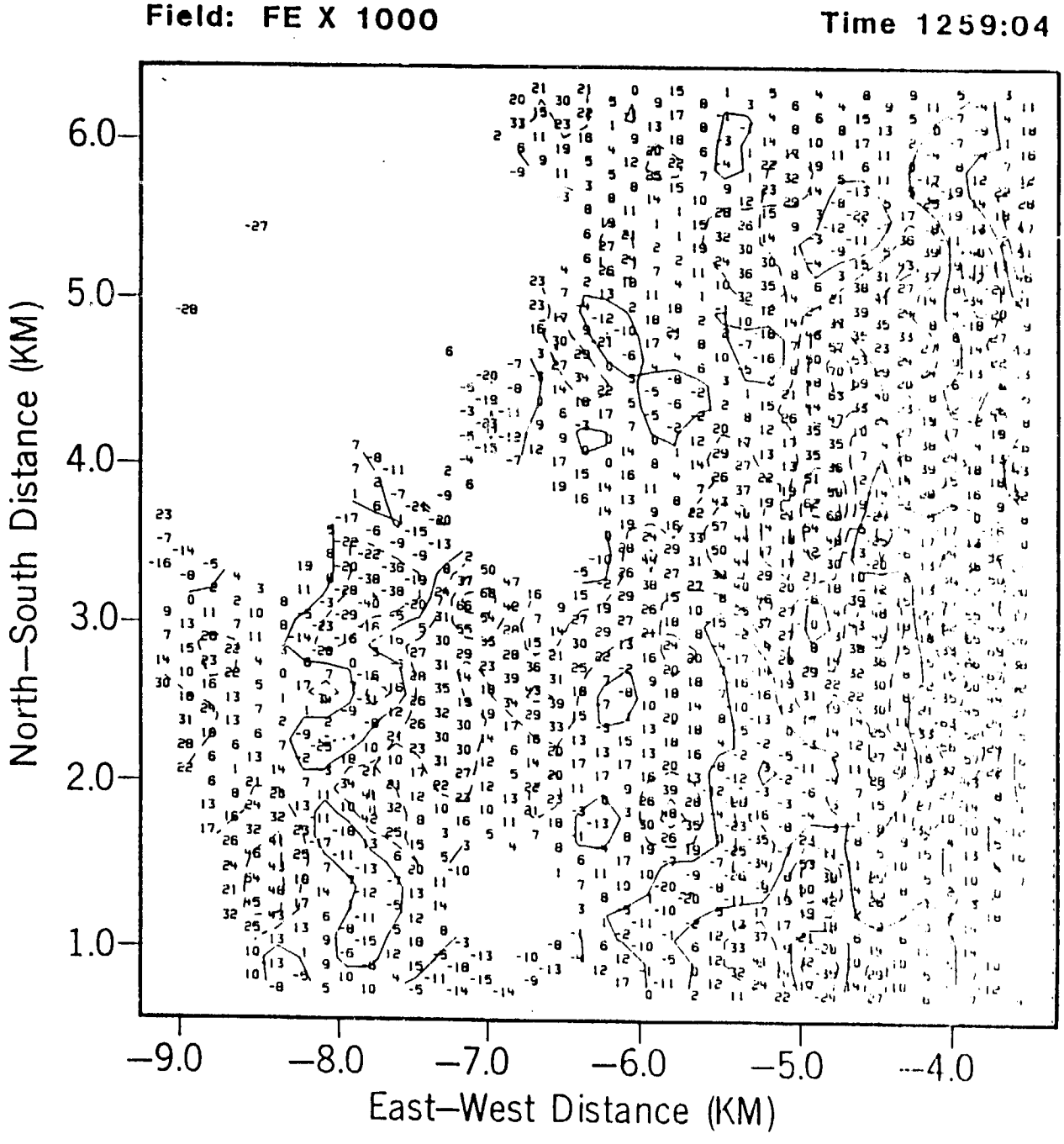

Reproduced from
best available copy.

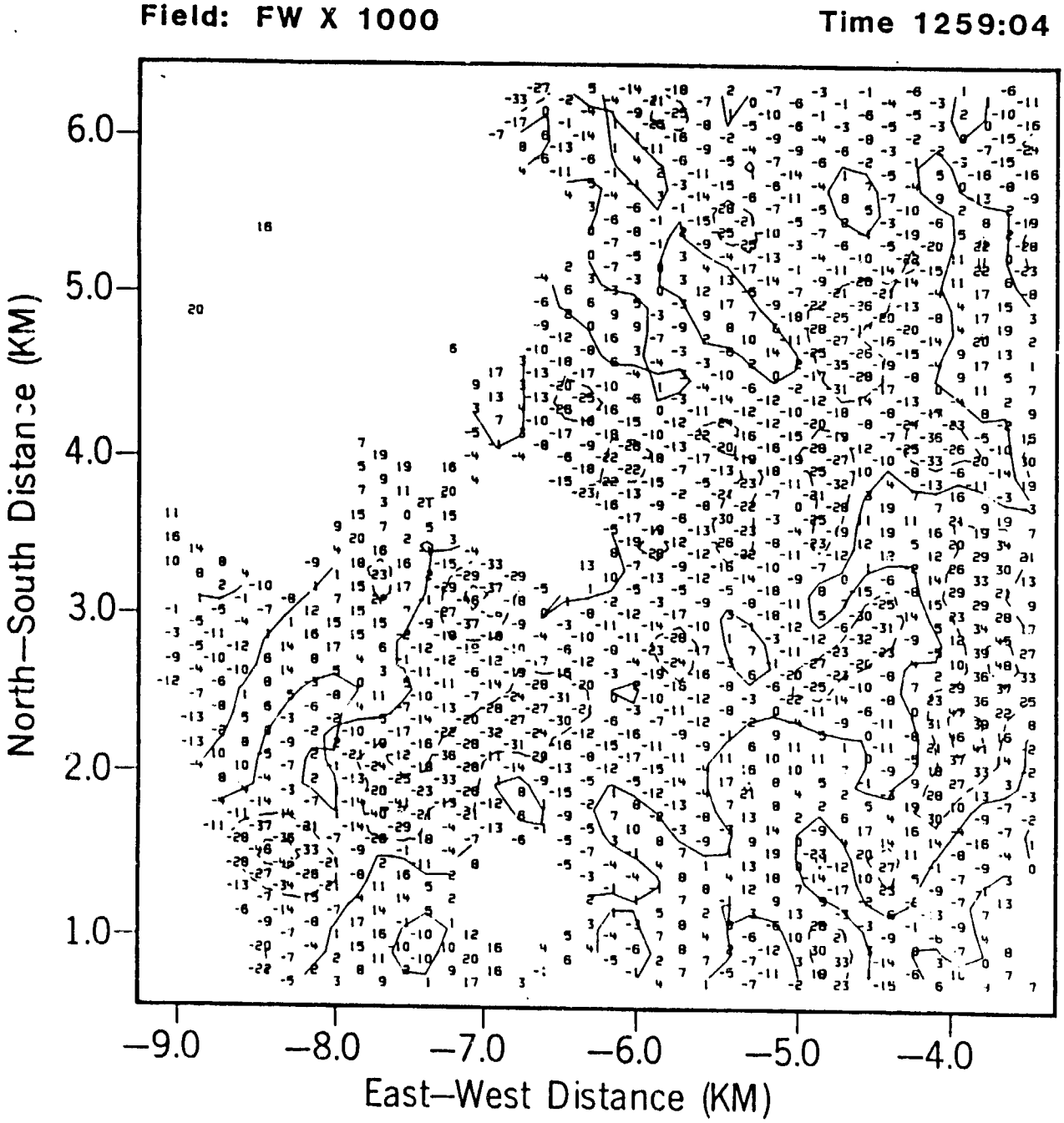
Field: FW X 1000
Time 1259:04
6.0
5.0
4.0
3.0
2.0
1.0
North—South Distance (KM)
—9.0
—8.0
—7.0
—6.0
—5.0
—4.0
East—West Distance (KM)

APPENDIX III

Tape Format

```
                                TAPE HEADER
CARD IMAGE FORMAT (80 ASCII CHARACTERS/RECORD)
STRUCTURE
   TAPE HEADER
   [EOF]

   VOLUME HEADER (VOLUME 1)
   LINE 1 FORMAT(11X,A10,11X,A5,19X,F10.3)
      TAPE NAME (A10) SCAN MODE (A5) MISSING DATA FLAG (F10.3)
   LINE 2 FORMAT(13X,A10,15X,I3,15X,I3,I5)
      VOLUME NAME (A10) VOLUME NUMBER (I3) PHYSICAL FILE (I3)(I5) FILES IN VOLM
   LINE 3 FORMAT(19X,2I7,11X,2I7)
       VOLUME BEGIN TIME ( YYMMDD HHMMSS)  END TIME (2I7)
   LINE 4 FORMAT(A)
      TITLE FOR LINES 5 THRU 7
   LINES 5-7 FORMAT(16X,A1,I6,3F10.3,A3,I7)
      THESE LINES CONTAIN THE VOLUME COORDINATES (A1), COORDINATE INDICES (I6),
      LIMITS, INCREMENT (3F10.3) AND DIMENSION (I7)
      FOR EACH INDEX
   LINE 8 FORMAT(15X,I2,28X,I8)
      NUMBER FIELDS (I2)  NUMBER POINTS/FIELD/PLANE (I8)
   LINE 9 FORMAT(A)
      FIELD NAMES IN SAME ORDER ON TAPE
   LINE 10 FORMAT(1X,8A10)
      10 CHARACTER FIELD NAMES
   LINE 11 FORMAT(17X,I2)
      NUMBERS OF RADARS (I2)
   LINE 12 FORMAT(A)
      RADAR COORDINATES
   LINES 13 TO EOF FORMAT(7X,I2,3F8.3)
      THESE LINES CONTAIN RADAR NUMBER AND COORDINATES(X,Y,Z) FOR EACH RADAR
   [EOF]

   EACH PLANE OF THE VOLUME IS WRITTEN IN A SEPARATE FILE
   LINE 1 IS A FILE HEADER   FORMAT(1X,2A10,F10.3,5I8)
   CONTENTS OF FILE HEADER
      TAPE NAME (A10)
      VOLUME NAME (A10)
      LEVEL OF PLANE (X,Y, OR Z) IN KM (F10.3)
      NUMBER OF PLANES (FILES) IN VOLUME (I8)
      PLANE (FILE) NUMBER THIS VOLUME (I8)
      NUMBER OF FIELDS IN VOLUME (I8)
      NUMBER OF POINTS/FIELD IN PLANE (I8)
      PHYSICAL FILE NUMBER (I8)

   THE FILE HEADER IS FOLLOWED BY THE FIRST FIELD FOR THIS PLANE.  THE NUMBER OF
   POINTS AND THE DIMENSIONS ARE GIVEN IN THE VOLUME HEADER.
   THE DATA ARE WRITTEN WITH FORMAT(1X,6E13.6).

   ALL FIELDS ARE WRITTEN CONSECUTIVELY IN THE ORDER GIVEN IN THE VOLUME HEADER
   AND EACH FIELD BEGINS A NEW RECORD.

   THE REST OF THE TAPE IS AS FOLLOWS
   [EOF]
   FILE HEADER (PLANE 2)
   DATA ALL FIELDS
   [EOF]
   FILE HEADER (PLANE 3)



   [EOF]
   VOLUME HEADER (VOLUME 2)
```

```
TAPE NAME              SCAN MODE CRT    MISSING DATA FLAG          .000
VOLUME NAME M311247     VOLUME NUMBER    1 PHYSICAL FILE   1     4 FILES IN VOLM
VOLUME BEGIN TIME  840531 124723  END TIME  840531 124725
VOLUME COORDINATE INDEX       MIN          MAX   INCREMENT     NUMBER
                X      1     -9.225      -3.375       .150 KM      40
                Y      2       .575       6.425       .150 KM      40
                Z      3       .075        .525       .150 KM       4
NUMBER FIELDS  4  NUMBER POINTS/FIELD/PLANE      1600
FIELD NAMES IN SAME ORDER ON TAPE
FN         FS         FE         FW
NUMBER OF RADARS 2
RADAR COORDINATES
 RADAR 1     .000     .000     .000
 RADAR 2     .790   -4.070     .020


TAPE NAME              SCAN MODE CRT    MISSING DATA FLAG          .000
VOLUME NAME M311249     VOLUME NUMBER    2 PHYSICAL FILE   6     4 FILES IN VOLM
VOLUME BEGIN TIME  840531 124903  END TIME  840531 124905
VOLUME COORDINATE INDEX       MIN          MAX   INCREMENT     NUMBER
                X      1     -9.225      -3.375       .150 KM      40
                Y      2       .575       6.425       .150 KM      40
                Z      3       .075        .525       .150 KM       4
NUMBER FIELDS  4  NUMBER POINTS/FIELD/PLANE      1600
FIELD NAMES IN SAME ORDER ON TAPE
FN         FS         FE         FW
NUMBER OF RADARS 2
RADAR COORDINATES
 RADAR 1     .000     .000     .000
 RADAR 2     .790   -4.070     .020


TAPE NAME              SCAN MODE CRT    MISSING DATA FLAG          .000
VOLUME NAME DREF1250    VOLUME NUMBER    3 PHYSICAL FILE  11     4 FILES IN VOLM
VOLUME BEGIN TIME  840531 125043  END TIME  840531 125043
VOLUME COORDINATE INDEX       MIN          MAX   INCREMENT     NUMBER
                X      1     -9.225      -3.375       .150 KM      40
                Y      2       .575       6.425       .150 KM      40
                Z      3       .075        .525       .150 KM       4
NUMBER FIELDS  4  NUMBER POINTS/FIELD/PLANE      1600
FIELD NAMES IN SAME ORDER ON TAPE
FN         FS         FE         FW
NUMBER OF RADARS 2
RADAR COORDINATES
 RADAR 1     .000     .000     .000
 RADAR 2    5.130    6.530    -.060


TAPE NAME              SCAN MODE CRT    MISSING DATA FLAG          .000
VOLUME NAME DREF1252    VOLUME NUMBER    4 PHYSICAL FILE  16     4 FILES IN VOLM
VOLUME BEGIN TIME  840531 125223  END TIME  840531 125223
VOLUME COORDINATE INDEX       MIN          MAX   INCREMENT     NUMBER
                X      1     -9.225      -3.375       .150 KM      40
                Y      2       .575       6.425       .150 KM      40
                Z      3       .075        .525       .150 KM       4
NUMBER FIELDS  4  NUMBER POINTS/FIELD/PLANE      1600
FIELD NAMES IN SAME ORDER ON TAPE
FN         FS         FE         FW
NUMBER OF RADARS 2
RADAR COORDINATES
 RADAR 1     .000     .000     .000
 RADAR 2    5.130    6.530    -.060
```

```
TAPE NAME              SCAN MODE CRT    MISSING DATA FLAG        .000
VOLUME NAME DREF1254   VOLUME NUMBER    5 PHYSICAL FILE  21     4 FILES IN VOLM
VOLUME BEGIN TIME  840531 125404  END TIME  840531 125404
VOLUME COORDINATE INDEX      MIN        MAX   INCREMENT     NUMBER
                  X     1    -9.225     -3.375      .150 KM      40
                  Y     2      .575      6.425      .150 KM      40
                  Z     3      .075       .525      .150 KM       4
NUMBER FIELDS  4  NUMBER POINTS/FIELD/PLANE      1600
FIELD NAMES IN SAME ORDER ON TAPE
FN        FS        FE        FW
NUMBER OF RADARS 2
RADAR COORDINATES
 RADAR 1     .000     .000     .000
 RADAR 2    5.130    6.530    -.060
```

```
TAPE NAME              SCAN MODE CRT    MISSING DATA FLAG        .000
VOLUME NAME DREF1255   VOLUME NUMBER    6 PHYSICAL FILE  26     4 FILES IN VOLM
VOLUME BEGIN TIME  840531 125544  END TIME  840531 125544
VOLUME COORDINATE INDEX      MIN        MAX   INCREMENT     NUMBER
                  X     1    -9.225     -3.375      .150 KM      40
                  Y     2      .575      6.425      .150 KM      40
                  Z     3      .075       .525      .150 KM       4
NUMBER FIELDS  4  NUMBER POINTS/FIELD/PLANE      1600
FIELD NAMES IN SAME ORDER ON TAPE
FN        FS        FE        FW
NUMBER OF RADARS 2
RADAR COORDINATES
 RADAR 1     .000     .000     .000
 RADAR 2    5.130    6.530    -.060
```

```
TAPE NAME              SCAN MODE CRT    MISSING DATA FLAG        .000
VOLUME NAME M311257    VOLUME NUMBER    7 PHYSICAL FILE  31     4 FILES IN VOLM
VOLUME BEGIN TIME  840531 125724  END TIME  840531 125727
VOLUME COORDINATE INDEX      MIN        MAX   INCREMENT     NUMBER
                  X     1    -9.225     -3.375      .150 KM      40
                  Y     2      .575      6.425      .150 KM      40
                  Z     3      .075       .525      .150 KM       4
NUMBER FIELDS  4  NUMBER POINTS/FIELD/PLANE      1600
FIELD NAMES IN SAME ORDER ON TAPE
FN        FS        FE        FW
NUMBER OF RADARS 2
RADAR COORDINATES
 RADAR 1     .000     .000     .000
 RADAR 2     .780   -6.070     .020
```

```
TAPE NAME              SCAN MODE CRT    MISSING DATA FLAG        .000
VOLUME NAME M311259    VOLUME NUMBER    8 PHYSICAL FILE  36     4 FILES IN VOLM
VOLUME BEGIN TIME  840531 125904  END TIME  840531 125907
VOLUME COORDINATE INDEX      MIN        MAX   INCREMENT     NUMBER
                  X     1    -9.225     -3.375      .150 KM      40
                  Y     2      .575      6.425      .150 KM      40
                  Z     3      .075       .525      .150 KM       4
NUMBER FIELDS  4  NUMBER POINTS/FIELD/PLANE      1600
FIELD NAMES IN SAME ORDER ON TAPE
FN        FS        FE        FW
NUMBER OF RADARS 2
RADAR COORDINATES
 RADAR 1     .000     .000     .000
 RADAR 2     .780   -6.070     .020
```